10-12-2017

Thermodynamics of concentrated solid solution alloys

Michael C. Gao
National Energy Transportation Laboratory

Chuan Zhang
CompuTherm LLC

Pan Gao
Tennessee State University

Fan Zhang
CompuTherm LLC

Lizhi Ouyang
Tennessee State University

See next page for additional authors

Recommended Citation

M.C. Gao, C. Zhang, P. Gao, F. Zhang, L.Z. Ouyang, M. Widom, J.A. Hawk, "Thermodynamics of concentrated solid solution alloys", Current Opinion in Solid State and Materials Science, Vol. 21, Issue 5, 2017, Pages 238-251, ISSN 1359-0286, https://doi.org/10.1016/j.cossms.2017.08.001.

Thermodynamics of Concentrated Solid Solution Alloys

M. C. Gao[1,2*], C. Zhang[3], P. Gao[4], F. Zhang[3], L.Z. Ouyang[4], M. Widom[5], and J. A. Hawk[1]

[1]National Energy Technology Laboratory, Albany, OR 97321, USA.

[2]AECOM, P.O. Box 1959, Albany, OR 97321, USA.

[3]CompuTherm LLC, Middleton, WI 53562, USA.

[4]Tennessee State University, Nashville, TN 37209, USA.

[5]Carnegie Mellon University, Pittsburgh, PA 15213, USA.

*****Correspondence: michael.gao@netl.doe.gov. Tel: +1-541-967-5869. Fax: +1-541-918-4493

Abstract

This paper reviews the three main approaches for predicting the formation of concentrated solid solution alloys (CSSA) and for modeling their thermodynamic properties, in particular, utilizing the methodologies of empirical thermo-physical parameters, CALPHAD method, and first-principles calculations combined with hybrid Monte Carlo/Molecular Dynamics (MC/MD) simulations. In order to speed up CSSA development, a variety of empirical parameters based on Hume-Rothery rules have been developed. Herein, these parameters have been systematically and critically evaluated for their efficiency in predicting solid solution formation. The phase stability of representative CSSA systems is then illustrated from the perspectives of phase diagrams and nucleation driving force plots of the σ phase using CALPHAD method. The temperature-dependent total entropies of the FCC, BCC, HCP, and σ phases in equimolar compositions of various systems are presented next, followed by the thermodynamic properties of mixing of the BCC phase in Al-containing and Ti-containing refractory metal systems. First-principles calculations on model FCC, BCC and HCP CSSA reveal the presence of both positive and negative vibrational entropies of mixing, while the calculated electronic entropies of mixing are negligible. Temperature dependent configurational entropy is determined from the atomic structures obtained from MC/MD simulations. Current status and challenges in using these methodologies as they pertain to thermodynamic property analysis and CSSA design are discussed.

1. Introduction

Traditional physical metallurgy has paid relatively little attention to multi-component concentrated solid solution alloys (CSSA) until Yeh [1] and Cantor [2] independently published their first papers on the subject in 2004. (Note: Yeh has named such alloys as “high-entropy alloys”, but for the sake of consistency only the term “CSSA” will be used in this paper.) Comprehensive reviews on the structures and properties of CSSA are provided in Refs. [3-5]. One important fundamental property of CSSA is the thermodynamics that governs their phase stability, which impacts the microstructure and

resulting mechanical, physical and environmental properties. The main objective of this paper is to provide a critical review on the prediction of CSSA formation and the modeling of thermodynamic properties of single-phase CSSA systems using three representative methodologies: (1) empirical thermo-physical parameters, (2) CALPHAD (acronym of CALculation of PHAse Diagrams) method, and (3) first-principles density functional theory (DFT) calculations combined with hybrid MC/MD simulations. Current status and the challenges in using these methodologies as they pertain to the thermodynamic evaluation and alloy design are also reviewed. Efficient strategies to accelerate the development of new CSSA by combining these methodologies will be discussed.

One important topic for thermodynamics of CSSA is predicting solid solution formation, given an arbitrary combination of metallic elements in the periodic table. Since the maximum ideal configurational entropy occurs at equimolar compositions (i.e., $S_{\max}^{conf} = R\ln N$, where N is the total number of components in the solution and R is the ideal gas constant), most studies on CSSA focus on equimolar or near equimolar compositions. Although increasing the number of principal components in the system has been claimed to potentially stabilize the solid solution against ordered intermetallic compounds, to date the vast majority of multicomponent CSSA published in the literature contain more than one phase in the microstructure (i.e., in the as-cast state or after annealing) [3, 6-8]. The presence of additional phases in the microstructure usually cause elemental partitioning among these phases, and thus, reduces the configurational entropy of the solid solution. The total number of single-phase CSSA reported in the literature is still very limited, and one possible reason may be lack of effective searching guidelines [9, 10]. Another reason for this could be that the entropy does not always dominate over enthalpy. For hitherto reported multicomponent CSSA in the literature, the alloys with the face-centered cubic (FCC) structure are mostly based on CoCrFeMnNi [2] and its derivatives. The alloys with the body-centered cubic (BCC) structure are mostly based on refractory metals [11, 12], while the alloys with the hexagonal closed-packed (HCP) structure are mostly based on either rare earth elements or late transition metals [10].

Various empirical thermo-physical parameters [7, 13-23] have been proposed in the literature to predict solid solution variants of CSSA, which originated from the Hume-Rothery rules. Due to lack of reliable phase diagrams for multicomponent CSSA systems, composition screening using this approach can be fast but at the cost of reliability. Ambiguity in defining single-phase solid solution alloys has cast doubt on some of empirical parameters. For example, many alloys that contain two FCC phases (e.g., coexistence of Cu-rich FCC phase with another FCC phase), or two BCC phases (e. g., coexistence of a BCC phase with another BCC phase or B2 phase), are counted as single-phase compositions [6, 13, 22-24]. Furthermore, some empirical rules have been determined based on limited number of compositions [16, 18, 21, 22]. In order to better understand the strengths and weaknesses of each set of empirical

parameters, this study collects and assesses the most up-to-date experimentally reported CSSA compositions with the FCC, BCC, HCP, multiphase, and amorphous structures (see Table S1), and evaluates the efficiency in predicting single-phase solid solutions. Alloys with two FCC or BCC phases in the microstructure are treated as multi-phase compositions. In addition, discrepancies in the atomic radii used by various research groups are also addressed. For consistency the atomic radii that corresponds to coordination number 12 are used here for metallic elements while the radii of tetrahedral covalent bonds are used for interstitial elements. These values are taken from Ref. [25]. Assessment of experimental reports in the literature and subsequent evaluation of the widely used empirical thermo-physical parameters used in predicting single-phase CSSA are presented in Section 2.

Contrasted to the use of empirical parameters is CALPHAD method [26, 27]. It is the most robust approach for predicting phase stability and it is the most effective way in calculating multi-component phase diagrams as long as a reliable thermodynamic database for the system under investigation is available. As a mature methodology, CALPHAD method has been applied to a broad range of materials science and engineering problems beyond just phase diagrams, including solidification, coating, joining, and phase transformation. In particular, applications of CALPHAD method to CSSA systems, using PanHEA [28], TCNI8 [29], and TTNI8 [29] databases, for materials design have been reported in Refs. [12, 30-35] with reasonable success. The applications of CALPHAD modeling to CSSA are detailed in Section 3. Phase diagrams for the Co-Cr-Fe-Mn-Ni system with varying number of components are developed, followed by nucleation driving force contour plots for the competing σ phase in the temperature-composition space of the various systems. Then the total entropies for the FCC, BCC, HCP and σ phases, as a function of composition and temperature, are presented. Finally, the entropies of mixing and enthalpies of mixing of BCC phases in Al-containing and Ti-containing CSSA systems are calculated to illustrate the concept of excess entropy.

First-principles DFT calculations prove to be very useful in providing physics-based thermo-chemistry data and for predicting phase equilibria without experimental input. The atomic structure, the phase stability, elasticity, electronic structure, magnetic property, and vibrational properties of multicomponent CSSA have been modeled using DFT [36-42]. Applications of DFT methods and hybrid Monte Carlo/Molecular Dynamics (MC/MD) simulations to predict the thermodynamic properties of CSSA are presented in Section 4. Enthalpies of formation of single-phase CSSA with the FCC, BCC and HCP structures at zero temperature are presented, followed by the entropy sources, in particular, from lattice vibration, electronic excitation and solid solution configuration. Such calculations are supplementary to CALPHAD modeling, and can also be used as input to CALPHAD database development.

Each of these approaches used in tackling the formation and thermodynamics of CSSA has its own strengths and weaknesses, and identifying the underlying hypotheses and potential pitfalls are important to rationally interpreting the results. This is covered in Section 5. In particular the roadblocks to developing reliable thermodynamic databases for multi-component CSSA systems, and accordingly the solution to them, are discussed in detail. For example, the lack of experimental data on phase equilibria and thermo-chemistry of multicomponent CSSA systems is addressed as is the importance in assigning physically meaningful energy data to those hypothetical phases (partially for the purpose of database compatibility), and integrating DFT energetics into CALPHAD as input.

2. Empirical thermo-physical parameters

Following the Hume–Rothery rules, various empirical thermo-physical parameters are proposed to predict CSSA formation. These parameters include ideal configurational entropy (S_{ideal}^{conf}), enthalpy of mixing in the liquid phase (ΔH_{mix}^{liq}) [13], atomic size difference (δ) [13], the Ω-parameter that is determined by $\overline{T_m} S_{ideal}^{conf} \Big/ \left|\Delta H_{mix}^{liq}\right|$ (where $\overline{T_m}$ is the composition-weighted average melting point) [7], valence electron concentration ($\overline{VEC}$) [14], electronegativity difference ($\Delta\chi$) [15], the ϕ-parameter [16] that defines the ratio of the difference between S_{ideal}^{conf} and the entropy at $\overline{T_m}$ over the phenomenological "excess entropy" that is calculated using atomic size and packing efficiency, elastic residual strain root mean square ($\varepsilon_{R.M.S.}$, or $\sqrt{\langle \varepsilon^2 \rangle}$) [17], the atomic size-related α_2-parameter [18], and intrinsic elastic strain energy (E_2 / E_0) [18]. The equations to calculate these parameters are compiled in Supplementary Materials. Commonly accepted criteria based on these parameters to form single-phase CSSA are: -15 kJ/mol $\leq \Delta H_{mix}^{liq} \leq$ +5 kJ/mol, $\delta \leq 6.6\%$, $\Omega \geq 1.1$, $\varepsilon_{R.M.S.} \leq 0.05$, and $\phi \geq 20$.

More sophisticated empirical models that compare the free energies (enthalpy and entropy) of both the solid solution phase and the intermetallic compound are also proposed, which include the Φ–parameter [19], η–parameter [20], and the κ_1^{cr} parameter [21]. These oversimplified models only consider one hypothetical solid solution phase and one hypothetical intermetallic compound at the nominal composition. The hypothesis for these models is that, in order to form a solid solution, the free energy of the hypothetical solid solution must be more negative than that of the hypothetical intermetallic compound at any given temperature. However, this hypothesis is not true for multicomponent alloys because solid-state phase equilibria for multi-component systems usually involve multiple phases (potentially three or more) at a given temperature. In fact, phase stability in CSSA systems at constant temperature and pressure is determined by minimizing the Gibbs free energy of the system ($G^{\varphi} = H^{\varphi} -$

TS^{φ} for single phase φ, where H is enthalpy and S is entropy; $G = f_i \sum_i^N G^i$ for multiphase systems, where f_i is the molar fraction of phase *i*).

The proposed criteria to form a single-phase solid solution using the free energy model are $\Phi \geq 1$ [19], $\eta \geq 1$ [20], and $\Delta H_{IM}/\Delta H_{mix}^{liq} < \kappa_1^{cr}$ [21]. Here ΔH_{IM} refers to the composition-weighted average enthalpy of formation of the most stable constituent binary intermetallic compounds (ΔH_{ij}^{IM}) that are taken from DFT data in the literature. The Φ–parameter is defined as the absolute value of the ratio of the Gibbs free energy of solid solution phase over that of the intermetallic compound. The enthalpy for both the solid solution and the compound phases are derived using the Miedema model [43] while ignoring the entropy of the compound. The η–parameter [20] is determined by $-T_{ann} S_{ideal}^{conf} \big/ |\Delta H_{ij}^{IM}|^{\max}$. Here an annealing temperature (T_{ann}) defines the temperature where annealing experiments are usually performed to reach homogeneous microstructure. The κ_1^{cr} parameter is determined by $1 - T_{ann}\left(S_{ideal}^{conf} - \Delta S_{IM}\right)\big/\Delta H_{mix}^{liq}$ (here ΔS_{IM} represents the entropy of an intermetallic compound). Although the entropy of intermetallic compounds can vary in a wide range depending on its crystal structure and constituent elements, Senkov and Miracle [21] assigned it to be a fraction (e.g., 0.6) of S_{ideal}^{conf}, for the sake of simplicity.

Figure 1 compares the effectiveness of various empirical rules. The $\Delta H_{mix}^{liq} - \delta$ relation (Fig. 1a) appears to be very powerful. All single-phase compositions are located within the region $\delta \leq 6.1\%$ and -16 kJ/mol $\leq \Delta H_{mix}^{liq} <$ +5 kJ/mol, while all the amorphous and a fraction of the multiphase compositions are located outside the region. However, this criterion is not a sufficient requirement since the region also contains most of the multiphase compositions. Similarly, the Ω–parameter (Fig. 1b) is useful in separating single-phase compositions from amorphous compositions with the threshold value of 1.0–1.1, but most multiphase compositions also possess $\Omega \geq 1.1$. In contrast, the $\Delta\chi$ parameter (Fig. 1b) is not quite as effective since for alloys below 0.44 significant scatter is observed. Figure 1c shows a threshold value of 0.19 rather than 1.0 for the η-parameter derived from Ref. [20], and a threshold value of 7.0 rather than 20 for ϕ-parameter [16]. Note that neither $\eta \geq 0.19$ nor $\phi \geq 7.0$ are sufficient conditions for forming solid solutions. However, combining these parameters proves to be much more effective than using them alone (Fig. 1c). Alternatively, the $\Delta H_{IM}/\Delta H_{mix}^{liq} < \kappa_1^{cr}$ relation (Fig. 1d) separates the vast majority of multiphase compositions from single-phase compositions. However, exceptions do occur. Many amorphous compositions are located in the same region as most single-phase alloys, and about a dozen single-phase and multiphase compositions fail to meet the criteria of these relations as well. The

elastic strain energy-residual strain *vs*. residual strain (Fig. 1e) indicates that $\varepsilon_{R.M.S.} \leq 6.1\%$ or $E_2 / E_0 \leq 13.6\times10^{-4}$ promotes the formation of a single-phase solid solution, but considerable overlap exists between multiphase and single-phase compositions, suggesting that both are necessary, but not sufficient, conditions in forming a solid solution. Note that the $\varepsilon_{R.M.S.}$ and δ values are almost equivalent (see Table S1) and indeed both involve only atomic sizes.

In order to predict the crystal structure type of a solid solution, Guo et al. [14] first proposed the $\overline{VEC}$ criterion. They claimed that FCC phases form at high $\overline{VEC}$ (> 8), BCC phases form at low $\overline{VEC}$ (< 6.87), and FCC + BCC phases form at intermediate $\overline{VEC}$ (6.87–8). As Fig. 1f shows, the threshold $\overline{VEC}$ identified in this study differs slightly from Ref. [14]. That is, FCC alloys are found to have $\overline{VEC} \geq 7.8$, and BCC alloys have $\overline{VEC} < 6$. Rare-earth HCP alloys have $\overline{VEC}$ of 3, while transition-metal HCP alloys have $\overline{VEC}$ about 7.5–8.5. Although the $\overline{VEC}$ criterion can serve as a useful guide for predicting the structure type of a solid solution, it cannot be used to predict whether or not solid solution will form. For example, no threshold $\overline{VEC}$ could be established for multiphase and amorphous alloys. Note that most multiphase alloys have fairly high ΔS_{ideal}^{conf} ($\geq$ 14 J/K/mol, Fig. 1f), and no pattern can be identified between the phases and ΔS_{ideal}^{conf}. This suggests that high configurational entropy does not necessarily, at least not always, lead to formation of single-phase solid solution because entropy does not always dominate the contribution to the Gibbs free energy of a system. The solid solution entropy may be less than ideal, and additionally the coexisting phases themselves may lead to the minimum Gibbs energy of the system at a given temperature, pressure and bulk composition.

3. CALPHAD modeling: Phase diagrams, driving forces, and thermodynamic properties

The highly studied FCC CoCrFeMnNi alloy was discovered by Cantor et al. [2] who investigated two equi-molar alloys with 20 and 16 components. These alloys contained multiple phases and were brittle in the as-cast and as-melt-spun states. Since then, many reports studied the phase stability and microstructure of the CoCrFeMnNi alloy [44, 45] and its sub-system alloys [46, 47]. For example, Otto et al. [44] confirmed that a single FCC solid solution formed only in CoCrFeMnNi while five other alloys (i.e., CoCrCuFeMn, CoCrMnNiV, CoFeMnMoNi, CoFeMnNiV and CrFeMnNiTi) consisted of more than one phase after annealing at 1273 K or at 1123 K for 3 days. It is noteworthy that the experimental observation by Otto et al. [44] is reasonably well reproduced by CALPHAD modeling [8]. Many reported CSSAs with the major FCC phase in the microstructure are derivatives of the Co-Cr-Fe-Mn-Ni system, and were developed by adding (or replacing) elements, such as, Al_xCoCrCuFeNi [48, 49],

$Al_xCo_{1.5}CrFeNi_{1.5}Ti_y$ [50], $Al_xCoCrFeNi$ [34, 51, 52], CoCrCuFeNi [53], $CoCrFeNiNb_x$ [54], $CoCrFeNiMo_x$ [55] and $CoCrFeMnNiV_x$ [56]. Single phase FCC CSSA with four or more principal components are very limited [8, 57]. For example, adding Cu causes formation of a Cu-rich FCC phase [48, 49, 53], while adding Al promotes the formation of BCC and B2 phases [34, 48, 49, 51, 52]. In addition, if Ti is added in large amount to this CSSA, precipitation of other intermetallic compounds occurs [50, 58]. The FCC phase in CoCrFeMnNi and its sub-systems are very ductile. Precipitation of second phases usually enhance the strength of the alloy but leads to reduced ductility.

The phase stability of the Co-Cr-Fe-Mn-Ni, Al-Co-Cr-Fe-Ni and Co-Cr-Cu-Fe-Ni systems were modeled using the PanHEA database via the Pandat^{TM} software [28], and selected isopleths are shown in Figure 2. The database covers the complete descriptions of the constituent binary and ternary systems of the Al-Co-Cr-Cu-Fe-Mn-Ni-Si-Ti-Zr system [33, 34]. While Cr still acts as a strong BCC stabilizer in this system (Fig. 2a), the FCC phase has unusually large Cr solubility (close to ~30 at. %). This is primarily due to the entropy stabilization effect. Similar to its role in steels Ni behaves as potent FCC stabilizer in this system (Fig. 2b). Conversely, the FCC phase has very small solubility for Al (Fig. 2c) due to the large elastic strain energy of hosting Al atoms in the FCC lattice of 3d transition metals (TM) and the tendency to form extremely stable Al-TM intermetallic compounds [59]. Although Cu has an FCC crystal structure and has very similar atomic radius to that of other 3d TM, the mutual solubility between Cu and TM (except Ni and Mn) is very small due to their inherent repulsive interaction. As a result, Cu solubility in $CoCrCu_xFeNi$ is limited to ~8% (Fig. 2d). The calculated phase diagrams (Fig. 2) agree well with experiments [34, 51-53] at least at higher temperatures.

In CALPHAD phase diagrams are calculated by minimizing the Gibbs free energy of the system at given temperature and pressure. Typical phase diagrams show the most stable phases at varying temperature, pressure, and composition, while the driving force diagram shows the nucleation driving force of forming one "child" phase from the "parent" phase in the temperature-composition space. One main intermetallic compound competing against the FCC solid solution in the Co-Cr-Fe-Mn-Ni system is the σ phase that has Pearson symbol tP30 and space group $P4_2/mnm$ with prototype $Cr_{0.49}Fe_{0.51}$. Precipitation of the σ phase in the CoCrFeMnNi alloy after annealing at 973 K for 500 days is reported in Ref. [45], which has a composition: 18.1% Co, 46.8% Cr, 16.9% Fe, 12.5% Mn, and 5.7% Ni.

Figure 3 shows the nucleation driving force contour lines of forming σ phase from the FCC phase in the binary Co-Cr system, ternary CoFe-Cr section, quaternary CoFeMn-Cr section, and quinary CoFeMnNi-Cr section. During these calculations, only the FCC phase is set "active" while the σ phase is set "dormant"; all other phases are suspended. The area represented by green lines has negative driving

force, i.e., σ phase will not form. The area represented by red lines has positive driving force, i.e., σ phase can form. The larger the positive value, the higher the driving force to form the σ phase from the FCC phase. The calculations indicate that driving force to form σ phase from FCC is strong in the Co-Cr binary (Fig. 3a), but decreases with increasing configurational entropy of the systems, namely, CoFe-Cr, CoFeMn-Cr, and CoFeMnNi-Cr sections (Fig. 3b-d). This demonstrates that increasing entropy can decrease the nucleation driving force of intermetallic compounds. Driving force contour lines can also be plotted in a phase diagram to show the driving force of forming a certain phase (referred to as the stable phases), as shown in Figure S1 (Supplementary Materials).

The total entropies of the FCC, BCC, HCP and σ phases are shown in Figure 4 for equimolar compositions of CoCr, CoCrFe, CoCrFeMn, and CoCrFeMnNi. The default stable structures at 1 atm and 298.15 K are used as reference (i.e., Co – HCP, Cr – BCC, Fe – BCC, Mn – CBCC_A12, and Ni – FCC). The total entropy of each phase increases monotonically with increasing the number of components, reflecting the contribution from configurational entropy. They also increase with increasing temperature, indicating dominant contribution from vibrational entropy. Keep in mind that the ideal configurational entropies for equimolar binary, ternary, quaternary and quinary solid solution alloys are 5.8, 9.1, 11.5, and 13.4 J/K/mol, respectively, and they only constitute a small fraction of the total entropy. This agrees with other reports [41, 60].

Due to presence of short range order, or segregation, and the contribution from lattice phonon vibration, or magnetic contribution, the total entropy of mixing (ΔS_{mix}^{φ}) for a CSSA may not always follow ideal mixing and can cause positive or negative deviation from $-R\sum_i c_i \ln c_i$ (i.e., excess entropy). The excess entropy ($^{ex}S_{mix}^{\varphi}$) of a solution phase (φ) is calculated by subtracting the ideal configurational entropy from the total entropy of the alloy (ΔS_{mix}^{φ}) [33]: $^{ex}S_{mix}^{\varphi} = \Delta S_{mix}^{\varphi} + R\sum_i c_i \ln c_i$. The CALPHAD analysis on the thermodynamic properties of mixing for the FCC phase in the Co-Cr-Fe-Mn-Ni system at 1273 K by Zhang and Gao [33] using TCNI8 database [29] reveals positive excess entropy for binary Co-Cr and pseudo-binary CoFe-Cr, CoFeNi-Cr, and CoFeMnNi-Cr systems.

The thermodynamic properties of mixing for the BCC phase at 1273 K for Al-containing systems (Fig. 5a and 5b) and Ti-containing systems (Fig. 5c and 5d) were calculated by Rui et al. [61] using TCNI8 database. The results reveal significant negative excess entropy for those equimolar compositions (Fig. 5a). The calculated ΔS_{mix}^{BCC} at 1273 K are −4, −2, +2, +3, +6, and +10 J/(mol·K) for equimolar AlTi,

AlNb, AlNbTi, AlTiV, AlNbTiV, and AlCrNbTiV, respectively. The ideal configurational entropies are +6, +9, +12 and +13 J/(mol·K) for equimolar binary, ternary, quaternary and quinary compositions, respectively. In contrast, the excess entropy is predicted to be negligible in refractory CSSA systems when Al is absent (i.e., $CrTi_x$, $CrVTi_x$, $CrNbVTi_x$ and $CrNbVZrTi_x$ systems; see Fig. 5c). The strong attractive interatomic interaction between Al and transition metals [61] also causes very large negative values of enthalpy of mixing (ΔH_{mix}^{BCC}), as shown in Fig. 5b, and reducing Al contents results in much less negative ΔH_{mix}^{BCC}. Conversely, absence of Al in the refractory metal systems corresponds to greatly reduced $|\Delta H_{mix}^{BCC}|$ values (Fig. 5d). The ΔH_{mix}^{BCC} values are positive for $CrTi_x$, $CrVTi_x$, $CrNbVTi_x$ and $CrNbVZrTi_x$ systems except Ti-poor $CrVTi_x$ compositions, implying overall repulsive interactions for these compositions. Note that all these predictions obtained from CALPHAD method are subject to experimental verification and/or confirmation from DFT calculations in the future, and improvement to the database will enhance the reliability of these and subsequent calculations.

4. DFT calculations and hybrid MC/MD simulations: Entropy sources

For a long time the CSSA community has approximated the total entropy of mixing for a multicomponent CSSA to be the ideal configurational entropy. The exact values are not known for both the true configurational entropy and total entropy of mixing except a few recent theoretical reports [40, 41]. As such this section mainly focuses on predicting enthalpy of formation of solid solution (ΔH_{SS}), and more importantly, predicting the entropy sources of example CSSA compositions using DFT and MC/MD simulations. The DFT calculations were performed using VASP (Vienna Ab Initio Simulation Package) [62, 63], and details on the VASP settings are provided elsewhere [40, 41]. The input atomic structures for equimolar quaternary CSSA are taken from the special quasi-random structure (SQS) reported in Ref. [41]: the 64-atom SQS models for quaternary compositions, the 160-atom SQS model for quinary HCP alloys, and the 125-atom SQS models for quinary FCC and BCC alloys. The calculated ΔH_{SS} of widely studied single-phase CSSA are shown in Fig. 6, which are obtained from one SQS configuration per alloy composition. Prior study by Gao et al. [41] shows that the fluctuation in ΔH_{SS} due to the variation in the atomic configuration are relatively small, at least for the CoOsReRu, CoCrFeNi, and MoNbTaW alloys, and the averaged ΔH_{SS} are 2.724 ± 0.49, 8.354 ± 0.266, and -7.407 ± 0.069 kJ/mol, respectively.

In general, the total entropy of a solid solution phase may consist of the contributions from lattice vibration (S^{vib}), configuration (S^{conf}), electron excitation (S^{elec}), and magnetic spin fluctuations (S^{mag}):

$$S^{total} = S^{vib} + S^{conf} + S^{elec} + S^{mag}. \quad (1)$$

The entropy sources are temperature and volume dependent. It is assumed that the magnetic entropy term to FCC CoCrFeNi and CoCrFeMnNi should be small at T ≥ 293 K because their critical magnetic ordering temperatures are well below room temperature [64, 65]. No magnetism is reported for those refractory BCC multicomponent CSSAs. The vibrational entropy (S^{vib}) is calculated by:

$$S^{vib}(V,T) = 3k_B \int_0^{\infty} n^{vib}[(f_{BE}+1)\ln(f_{BE}+1) - f_{BE}\ln f_{BE}]d\varepsilon\,, \quad (2)$$

where n^{vib} is the phonon density of states, and f_{BE} is the Bose-Einstein distribution function. Phonon frequencies of the CSSA were calculated using the harmonic approximation by diagonalizing the dynamical matrix based on the interatomic force constants reported by VASP. The quasi-harmonic approximation can improve the accuracy at high temperatures, and more importantly, can predict the coefficient of thermal expansion. For a comprehensive review on the lattice vibration of crystalline solids, readers can refer to the work by Fultz [60].

Electronic excitation across the Fermi level by migrating from valance band to conduction band gives rise to electronic entropy (S^{elec}), which can be determined by:

$$S^{elec}(V,T) = -2k_B \int_{-\infty}^{\infty} n^{elec}\left[f_{FD}\ln f_{FD} + (1-f_{FD})\ln(1\text{-}f_{FD})\right]d\varepsilon, \quad (3)$$

where n^{elec} is the electron density of states, and f_{FD} is Fermi-Dirac distribution function.

For a solid solution as the temperature decreases, chemical ordering or phase separation sets in, which reduces the configurational entropy. At zero temperature, all entropy sources should vanish according to the Third Law of Thermodynamics. Such examples are shown in refractory CSSA by Widom et al. [37, 40] using hybrid MC/MD simulations. The canonical ensemble (NVT) (i.e., constant amount of substance, volume and temperature) was adopted for the FCC and BCC structures, and the isothermal-isobaric ensemble (NPT) (i.e., constant amount of substance, pressure and temperature) for the HCP structure. The supercells used in the present study contain 108, 128, and 96 atoms for FCC CoCrFeNi, BCC MoNbTaW, and HCP CoOsReRu, respectively. The simulations were done by alternating molecular dynamics at each temperature with Monte Carlo swaps, each performed from first principles using VASP. Monte Carlo swaps of atomic species on different sites are always accepted if the swap reduces the energy ($\Delta E = E_{swap} - E_{initial} < 0$; E_{swap} and $E_{initial}$ are the energies in the swapped and initial configurations, respectively). For those swaps that increase the energy ($\Delta E > 0$), the acceptance is determined by assessing the probability, $P = \exp(-\Delta E / k_B T)$. The energy barrier separating the swapped

and initial states are not relevant for Monte Carlo simulations and thus not considered. More details on the procedures are provided elsewhere [37, 40, 66]. The reduction in configurational entropy due to short-range chemical order can be calculated using the Guggenheim quasichemical model [67, 68], Bethe lattice [69], or Kikuchi cluster variation method (CVM) [70]. Specifically, the reduction in entropy due to near neighbor correlations (y_{ij}) using Kikuchi CVM is calculated by:

$$I = \sum_{i,j=1}^{N} y_{ij} ln\left(y_{ij}/c_i c_j\right) \quad (4)$$

where c_i and c_j are the mole fraction of elements *i* and *j*, respectively.

Figure 7 compares the vibrational, electronic, and configurational entropies for three model CSSAs: (1) FCC CoCrFeNi, (2) BCC MoNbTaW, and (3) HCP CoOsReRu. Note that the vibrational entropy of BCC Cr was used here because of presence of 64 imaginary vibrational modes and the elastic instability for FCC Cr. The vibrational entropy is very similar for MoNbTaW and CoOsReRu (as expected due to their similar average masses), but it is slightly smaller for CoCrFeNi (also as expected due to its lower atomic mass). This is shown in Fig. 7a. Vibrational entropy is sensitive to temperature. It vanishes at zero temperature and increases rapidly with increasing temperature. Note that the vibrational entropies for the three alloys are already ~2.5 times the ideal configurational entropy at T = 300 K (Fig. 7a).

In contrast, the electronic entropy is small for all three compositions even at high temperatures (Fig. 7b). Configurational entropies (S^{conf}) for these alloys are fairly close to their ideal value (R ln 4) at temperatures close to the solidus temperatures, and start to decrease very gradually until the temperature reaches 1100 K (Fig.7c). At this point S^{conf} decreases rapidly, signaling the development of chemical short-range order in the alloys. Note that S^{conf} at room temperature is much lower for MoNbTaW than the others due to the tendency in forming the ordered BCC (i.e., B2) as revealed by Widom et al. [37, 66]. The total entropies (i.e., the sum of vibrational, electronic, and configurational entropy) of these alloys are shown in Fig. 7d. S^{total} is equivalent for MoNbTaV and CoOsReRu, and is greater than CoCrFeNi, following the same trend as seen for vibrational entropy (Fig. 7a).

Alloy entropies of mixing are determined as:

$$\Delta S_{mix} = S_{alloy} - \sum_{i=1}^{N} c_i S_i \quad (5)$$

where S_i is the entropy (total, vibrational, etc.) of the i^{th} element, c_i is the molar composition of the i^{th} element, and N is the total number of elements in the CSSA. Note that the pure elements lack configurational entropy, and hence, $\Delta S_{mix}^{conf} = S_{alloy}^{conf}$.

Figure 8 compares the mixing, vibrational and electronic entropies for the three model alloys. The calculations predict that lattice vibration increases the total entropy of CoCrFeNi, while vibration decreases the total entropy of MoNbTaW (Fig. 8a). The ΔS_{mix}^{vib} values for the three cases are small relative to the individual S_{alloy}^{vib} because the alloy vibrational frequencies lie close to the average of the individual elements. Indeed, often $\Delta S_{mix}^{vib} < S^{conf}$, and ΔS_{mix}^{vib} is near zero for CoOsReRu. At temperatures above the Debye temperature (i.e., T ≥ ~400 K), the vibrational entropies of mixing approach constant values, namely, +2.8 J/K/mol, -3.6 J/K/mol and -0.4 J/K/mol for CoCrFeNi, MoNbTaW and CoOsReRu, respectively, because the heat capacities approach their classical limit at 3R. Note that the predicted ΔS_{mix}^{vib} of +2.8 J/K/mol for CoCrFeNi is in excellent agreement with the calculated excess entropy of +2.5 J/K/mol [33] at 1273 K using CALPHAD method. In contrast, ΔS_{mix}^{elec} values are close to zero (Fig. 8b). The total entropies of mixing (i.e., $\Delta S_{mix}^{vib} + \Delta S_{mix}^{elec} + S^{conf}$) are shown in Fig. 8c and correspond to, in descending order: CoCrFeNi > CoOsReRu > MoNbTaW.

The positive contribution of phonon vibration to the solid solution stabilization was also reported in the literature by Fultz and co-workers [60, 71, 72]. For example, Fultz et al. [71] measured ΔS_{mix}^{vib} to be +1.17, +1.67 and +1.78 J/K/mol for disordered BCC solid solution alloys $Fe_{70}Cr_{30}$, $Fe_{53}Cr_{47}$ and $Fe_{30}Cr_{70}$, respectively. Nagel et al. [72] found that the disordered FCC Cu_3Au has a higher vibrational entropy than the ordered $L1_2$ Cu_3Au by approximately +1.16 J/K/mol at high temperature. However, generally speaking it is not obvious whether chemical disordering causes positive or negative vibrational entropy of mixing, or whether a disordered alloy will exhibit greater vibrational entropy than its ordered form. The vibrational entropy of mixing of an alloy may depend on the crystal structure, bonding and enthalpy of the alloy, as well as the molar volumes and structures of the constituent elements.

5. Discussion and outlook

The three major approaches that are widely used to predict CSSA formation and analyze the underlying thermodynamic properties have been reviewed. Due to inherent hypotheses or limitations in each approach, they possess strengths and weakness. Accordingly, it is prudent not to overstate their predictive capability, especially when using empirical thermo-physical parameters alone. In the following

section the reasons that may lead to inaccuracies in predictions when using these empirical parameters will be discussed. Additionally, ways to overcome common issues in developing reliable physics-based thermodynamic databases for multi-component CSSA systems will also be explored.

5.1 Empirical parameters: Flaws and limitations

This critical re-evaluation of empirical thermo-physical parameters demonstrates that most parameters are efficient in separating single-phase compositions from amorphous compositions. In general, they fail to separate single-phase compositions from multiphase compositions. Considerable overlap between single-phase compositions and multiphase compositions requires that new parameters, or identification methodologies, be developed that are stricter and more effective. The necessary requirements needed (but not sufficient) to form single-phase solid solution identified in this work are: -16.25 kJ/mol $\leq \Delta H_{mix}^{liq} \leq$ +5 kJ/mol, $\delta \leq 6\%$, $\Omega \geq 1$, $\eta \geq 0.19$, $\phi \geq 7.0$, $\varepsilon_{R.M.S.} \leq 0.061$, and $E_2/E_0 \leq 13.6 \times 10^{-4}$. Although $\overline{VEC}$ by itself cannot be used to predict solid solution formation, $\overline{VEC}$ can be effective in separating BCC from FCC compositions. For example, the FCC phase forms when $\overline{VEC} \geq 7.8$, while BCC phase forms when $\overline{VEC} \leq 6.0$. Note that the threshold values identified in this work differ somewhat from those reported in the literature. This appears to be due to the different compositional spaces assessed as well as different values of atomic radii. As more reliable and verified experimental data emerge in the literature, the threshold values may become a range rather than a fixed value [61].

Besides bias due to the availability of experimental compositions, the empirical rules also suffer in other ways. Most empirical rules assign the enthalpy of mixing of the liquid as determined from the Miedema model to the solid solution phase, primarily due to lack of reliable enthalpy data for the solid solution phase for CSSA systems. It is known that the enthalpy values from Miedema models can differ significantly from experimental data for certain systems. Gao et al. [12] studied these empirical parameters and thermodynamic properties for sixteen refractory BCC CCSA and found that both the sign and absolute value of ΔH_{mix}^{BCC} are not necessarily in accord with ΔH_{mix}^{liq}. In this work nine alloys exhibit opposite sign while seven alloys show significant contrast in their absolute values.

Secondly, the true configurational entropy of solid solution may not always follow ideal mixing behavior, and the deviation can be substantial. Positive excess entropies were predicted for the FCC phase at 1273 K in Co-Cr-Fe-Mn-Ni system [33], and negative excess entropies for the BCC phase at 1273 K in Al-containing CSSA such as Al-Cr-Nb-Ti-V [61]. Similarly, the enthalpy of mixing for the solid solution phase cannot be ignored, especially for systems that exhibit strong tendency to form extremely stable intermetallic compounds (e.g., Al-containing CSSA) [61].

Lastly, the configurational entropy of intermetallic compounds can be very small if the compositional homogeneity range remains extremely small in the multicomponent systems. Otherwise, the configurational entropies, in general, cannot be ignored, as argued by Senkov and Miracle [21]. Therefore, future work is needed to differentiate compositions that will likely show appreciable compositional homogeneity so that the empirical rules can be modified accordingly.

Regardless of the subtle differences among those empirical thermo-physical rules, they share one common thermodynamic flaw: *The phase stability of a multicomponent system is not determined by the simple comparison of the Gibbs free energies of a hypothetical solid solution with a hypothetical compound phase. Rather, it is determined by the equilibrium condition that the chemical potential of each component should be equal in all phases (or equivalently, the alloy free energy should touch the convex hull of free energies of all competing phases).* Consequently, these rules cannot predict the equilibrium phases and their crystal structures of arbitrary alloys reliably, nor can they predict the temperature and pressure dependence of phase stability. In fact, the simple comparison of the Gibbs free energy at one composition to determine phase equilibria among phases is only valid for the unary system.

5.2 CALPHAD for CSSA systems: Issues and solutions

To overcome those defects to which there are no easy solutions within the framework of the empirical thermo-physical parameters, CALPHAD method proves to be the most direct solution to phase stability of multicomponent systems. In terms of CSSA, predicted solid solution formation is confirmed through experiments [73-77]. Screening is carried out to identify low-density equimolar compositions in single-phase solid solution [32, 78]. Furthermore, non-equilibrium solidification using Scheil model [79] is used to predict segregation behavior in the as-cast state [33, 73, 75-77, 80]. Quantitative analyses in enthalpy, entropy, and Gibbs free energy of CSSA are also presented in Refs. [12, 44, 75, 76]. However, all these CALPHAD modeling predictions are susceptible to the reliability of the thermodynamic databases.

The essence of CALPHAD approach for a multicomponent system is to develop reliable self-consistent thermodynamic descriptions of all constituent binary and ternary systems, by fitting experimentally determined thermochemistry and phase equilibria as well as DFT-predicted data. The description of a quaternary or higher-order system can be obtained via an extrapolation method from the binary and ternary systems [81], subject to further adjustment of the database in comparison to experiments [33]. However, extrapolation of binaries and ternaries into higher order systems may not always guarantee satisfactory agreement with experiments. For example, if there are new stable quaternary or higher-order phases, or if the descriptions for those unstable or hypothetical

phases/endmembers are so unphysical that cause their undesired over-stabilization or underestimated stability, then extrapolation may not work. Since CALPHAD itself is not a predictive methodology like DFT, the thermodynamic descriptions for all phases in the system must be pre-defined. In case there exist new quaternary or higher-order compound phases in the system, then their Gibbs free energy descriptions in CALPHAD framework must be determined first.

Developing thermodynamic databases for multicomponent CSSA systems requires that the database be valid for the *entire* composition range, whereas traditional alloys are only concerned about the compositions in the corner of a principal element. For example, development of 10-component CSSA system requires optimization over the *entire* composition ranges for 45 constituent binaries and 120 constituent ternaries. Moreover, to date complete ternary phase diagrams are still very limited in extent, and even some binary phase diagrams require further experimental study to better define them. For example, a recent DFT study by Widom [40] predicts the existence of stable C14 NbV_2 Laves phase at $T \leq 1100$ K in the binary Nb-V system. This prediction has yet to be confirmed by experiment. Element Tc has the HCP crystal structure, and it is intuitively expected that there will be large mutual solubility between Tc and several transition elements (such as Re, Ru, and Os). However, most of the binary phase diagrams pertaining to Tc are still unknown. Therefore, a *complete* database including 10 or more components is rarely available. For example, even though commercial thermodynamic databases developed for traditional alloys may contain greater than 20 components, they are not intended for CSSA use where compositions are located far away from the principal element corner. Individuals doing CCSA thermodynamic research should be aware that using the thermodynamic databases developed for traditional alloys with one principal element may lead to erroneous results.

Another main challenge in developing databases for multicomponent CSSA systems is the lack of reliable energy data for hypothetical phases and endmembers, as discussed in Ref. [33]. One example is the σ phase in the Al-Co-Cr-Cu-Fe-Mn-Ni-Ti system. For example, the σ phase is stable in the Co-Cr and Cr-Fe systems, but it is not stable for Al- or Cu-containing binaries. Their energies, however, should be physically meaningful, and need to be accounted for in the database for the sake of compatibility. The adopted sublattice model and the assigned energies for the corresponding endmembers have profound influence on the stability of the σ phase. For instance, both TCNI8 and PanHEA databases underestimate the precipitation temperature of the σ phase for CoCrFeMnNi (i.e., 867 K by the former and 624 K by the latter). Experiment has shown that σ phase precipitates at 973 K [45]. The predicted composition of σ phase also differs greatly from experiments [45, 82]. TCNI8 predicts a composition of σ phase at T = 773 K to be 5.3% Co - 37.2% Cr - 30.0% Fe - 26.3% Mn - 1.2% Ni; PanHEA on the other hand predicts a composition at T = 623 K to be 2.1% Co - 48.5% Cr - 20.5% Fe - 28.5% Mn - 0.4% Ni.

Another example is Laves phase (i.e., C14, C15 and C36) in refractory metal system (e.g., Al-Cr-Hf-Mo-Nb-Ta-Ti-V-W-Zr). Laves phase is stable in Cr-M binaries (where M = Hf, Nb, Ta, Ti, Zr), but is not stable in many other systems (e.g., Cr-M (M = V, Mo, W), Ti-M (M = Mo, Nb, Ta, V, W) and Al-containing binaries). How a physically meaningful energy is assigned to these hypothetical or unstable phases remains an open question in CALPHAD community. Ideally, their composition and temperature dependence should be provided as well. With recent progress in first-principles DFT calculations, the enthalpy of formation [83-89] and even Gibbs free energy for relevant compounds [40] can be predicted without experimental input. The application of these data to the hypothetical compounds in binary and ternary systems is particularly important for developing physically meaningful databases for CSSA systems.

Lastly, very few experiments are dedicated to phase equilibria [34, 45] or thermo-chemistry data of multicomponent CSSAs. The majority experiments on CSSA in the literature report only on the microstructure and properties of the alloys in the as-cast state. In this condition, alloys possess severe compositional and structural inhomogeneity in their microstructures. Proper homogenization/annealing is necessary to achieve an "equilibrium" state [90]. For example, Zhang et al. [34] annealed the $Al_{0.3}$CoCrFeNi at 973 K for 500 h and the $Al_{0.7}$CoCrFeNi alloy at 1523 K for 1000 h, and they obtained good agreement between CALPHAD prediction and experiments. The experiment by Otto et al. [45] that annealed the CoCrFeMnNi alloy at 1173 K, 973 K, and 773 K for 500 days provides valuable first-hand experimental data to show that a multicomponent CSSA is thermodynamically stable within a certain temperature range, and decomposes to multiphase structures at sufficiently low temperatures, similar to binary and ternary CSSA.

In terms of predicting solid solution formation in multicomponent systems, one feasible and effective approach would be to use a combination of phase diagram inspection [9, 12], empirical parameter screening [7, 13-21], CALPHAD screening [9, 10, 12, 30-32, 78, 91], first-principles DFT calculations [40], and *ab initio* molecular dynamics (AIMD) simulations [3, 8-10]. In fact, using this strategy, Gao [8] predicted hundreds of quaternary and higher-order equimolar compositions in the Dy-Er-Gd-Ho-Lu-Sc-Sm-Tb-Tm-Y, Ba-Ca-Eu-Sr-Yb, Mo-Nb-Ta-Ti-V-W, and Mo-Nb-Re-Ta-Ti-V-W systems. Although CALPHAD method is powerful in calculating phase diagrams, it relies on pre-determination of all phases in the system and their thermodynamic descriptions. Future work to accelerate developing physics-based thermo-chemistry data for numerous hypothetical, or unstable phases/endmembers, will contribute substantially in developing reliable thermodynamic databases for CSSA systems. Reliable experiments on phase equilibria and phase thermo-chemistry ternaries, and higher-order systems, are also critically important.

6. Conclusions

This work reviews the present status in predicting the formation of CSSA and modeling their thermodynamic properties, from the perspectives of empirical thermo-physical parameters, CALPHAD method, and first-principles calculations combined hybrid MC/MD simulations. The effectiveness of most empirical rules to predict solid solution formation has been critically evaluated in a systematic way. Applications of CALPHAD method to predict phase stability and visualize phase diagrams of CSSA systems were illustrated. Identifying entropy sources of three model CSSA using first-principles DFT were also presented. Challenges associated with using these methodologies as they pertained to thermodynamics property development and alloy design were reviewed, and the efficient strategies they engendered in designing new CSSA were discussed. The following conclusions were developed:

1. Most proposed empirical thermo-physical parameters except $\Delta\chi$ are efficient in separating single-phase compositions from amorphous compositions, but they fail to separate single-phase compositions from multiphase compositions. Considerable overlapping of single-phase compositions with multiphase compositions requires the development of new empirical parameters or methodologies that are stricter and more effective.

2. The necessary requirements needed to form single-phase solid solutions were identified in the present work are:

   $-16.25\ \text{kJ/mol} \le \Delta H_{mix}^{liq} \le +5\ \text{kJ/mol}$,

   $\delta \le 6\%,\ \Omega \ge 1,\ \eta \ge 0.19,\ \phi \ge 7.0$,

   $\varepsilon_{R.M.S.} \le 0.061$, and $E_2/E_0 \le 13.6 \times 10^{-4}$.

   However, they are not sufficient conditions.

3. $\overline{VEC}$ is effective in separating BCC from FCC compositions. The FCC phase forms when $\overline{VEC} \ge 7.8$, while the BCC phase forms when $\overline{VEC} \le 6.0$. However, $\overline{VEC}$ cannot solely be used to predict solid solution formation.

4. Using the PanHEA database, calculated isopleths of $CoCr_xFeMnNi$, $CoCrFeMnNi_x$, $Al_xCoCrFeMn$, and $CoCrCu_xFeMn$ agree with experiments at higher temperatures. The driving force for σ phase nucleation from the FCC phase in Co-Cr binary, CoFe-Cr, CoFeNi-Cr, and CoFeMnNi-Cr vertical

sections were shown, and the driving force decreased with increasing the number of principal components.

5. The PanHEA database predicts: For solid solution phases (FCC, BCC, and HCP) and σ compound, (1) the total entropy increased with increasing the number of principal components; and (2) configurational entropy constituted a very small fraction of the total entropy, as determined from equimolar CoCr, CoCrFe, CoCrFeMn, and CoCrFeMnNi alloys.

6. TCNI8 database predicts noticeable negative excess entropy ($^{ex}S_{mix}^{BCC}$) together with large negative ΔH_{mix}^{BCC} for the BCC phase in Al-containing systems (namely, $AlTi_x$, $AlVTi_x$, $AlNbVTi_x$ and $AlCrNbVTi_x$), in sharp contrast to non-Al-containing systems (namely, $CrTi_x$, $CrVTi_x$, $CrNbVTi_x$ and $CrNbVZrTi_x$).

7. DFT calculated enthalpy of formation of select single-phase multicomponent CSSA are: -7.3 kJ/mol $< \Delta H_f <$ +8.4 kJ/mol.

8. Vibrational entropy of FCC CoCrFeNi, BCC MoNbTaW and HCP CoOsReRu is ~2.5 times the ideal configurational entropy at room temperature. The contribution from electronic entropy is truly negligible. The total entropies are equivalent for MoNbTaV and CoOsReRu, and greater than CoCrFeNi, and follow the same trend as was seen for vibrational entropy.

9. Vibrational entropy of mixing is small compared to the ideal configurational entropy. At T > 400 K, the calculated vibrational entropy of mixing is +2.8, -3.6 and -0.3 J/K/mol for FCC CoCrFeNi, BCC MoNbTaW and HCP CoOsReRu, respectively. The total entropies of mixing (i.e., $\Delta S_{mix}^{vib} + \Delta S_{mix}^{elec} + S^{conf}$) were observed to trend in the following manner: CoCrFeNi > CoOsReRu > MoNbTaW.

10. DFT predicted ΔS_{mix}^{vib} equal to +2.8 J/K/mol for FCC CoCrFeNi, which is in excellent agreement with the calculated excess entropy of +2.5 J/K/mol [33] at 1273 K using CALPHAD method.

11. Calculated configurational entropies (S^{conf}) for CoCrFeNi, MoNbTaW and CoOsReRu alloys were fairly equivalent to their ideal value ($R \ln 4$) at temperatures close to their solidus temperatures. The calculated entropies then start to decrease very gradually till 1100 K. Rapid decrease in S^{conf} becomes more apparent at T < 1100 K, signaling development of chemical short-range order in the alloys.

Acknowledgements

This work was carried out in support of the Cross-Cutting Technologies Program at the National Energy Technology Laboratory (NETL) – Strategic Center for Coal, managed by Robert Romanosky (Technology Manager) and Charles Miller (Technology Monitor). The Research was executed through NETL's Office of Research and Development's Innovative Process Technologies (IPT) Field Work Proposal. Research performed by AECOM Staff was conducted under the RES contract DE-FE-0004000. L.Z. Ouyang acknowledges support by DE-FE-0011549 and DE-NA0002630. Work at Carnegie Mellon was supported under grant DE-SC0014506. M.C. Gao thanks Yifan Ye for kindly sharing his Matlab codes to calculate ϕ-parameter and $\varepsilon_{R.M.S.}$.

References

[1] Yeh JW, Chen SK, Lin SJ, Gan JY, Chin TS, Shun TT, et al. Nanostructured High-Entropy Alloys with Multiple Principal Elements: Novel Alloy Design Concepts and Outcomes. Adv Eng Mater. 2004;6:299-303.

[2] Cantor B, Chang ITH, Knight P, Vincent AJB. Microstructural development in equiatomic multicomponent alloys. Mater Sci Eng A. 2004;375–377:213-8.

[3] Zhang Y, Zuo TT, Tang Z, Gao MC, Dahmen KA, Liaw PK, et al. Microstructures and Properties of High-entropy Alloys. Prog Mater Sci. 2014;61:1-93.

[4] Gao MC, Yeh JW, Liaw PK, Zhang Y. High-Entropy Alloys: Fundamentals and Applications. 1st ed. Cham, Switzerland: Springer International Publishing; 2016.

[5] Miracle DB, Senkov ON. A critical review of high entropy alloys and related concepts. Acta Mater. 2017;122:448-511.

[6] Yang X, Zhang Y. Prediction of high-entropy stabilized solid-solution in multi-component alloys. Mater Chem Phys. 2012;132:233-8.

[7] Zhang Y, Lu ZP, Ma SG, Liaw PK, Tang Z, Cheng YQ, et al. Guidelines in predicting phase formation of high-entropy alloys. MRS Comm. 2014;4:57-62.

[8] Gao MC. Design of High-Entropy Alloys. In: Gao MC, Yeh JW, Liaw PK, Zhang Y, editors. High-Entropy Alloys: Fundamentals and Applications. 1st ed. Cham, Switzerland: Springer International Publishing; 2016. p. 369-98.

[9] Gao MC, Alman DE. Searching for Next Single-Phase High-Entropy Alloy Compositions. Entropy. 2013;15:4504-19.

[10] Gao MC, Zhang B, Guo SM, Qiao JW, Hawk JA. High-Entropy Alloys in Hexagonal Close Packed Structure. Metall Mater Trans A. 2016;47A:3322-32.

[11] Senkov ON, Wilks GB, Miracle DB, Chuang CP, Liaw PK. Refractory high-entropy alloys. Intermetallics. 2010;18:1758-65.

[12] Gao MC, Carney CS, Doğan ÖN, Jablonksi PD, Hawk JA, Alman DE. Design of Refractory High-Entropy Alloys. JOM. 2015;67:2653-69.

[13] Zhang Y, Zhou YJ, Lin JP, Chen GL, Liaw PK. Solid-Solution Phase Formation Rules for Multi-component Alloys. Adv Eng Mater. 2008;10:534-8.

[14] Guo S, Ng C, Lu J, Liu CT. Effect of valence electron concentration on stability of fcc or bcc phase in high entropy alloys J Appl Phys. 2011;109:103505.

[15] Fang S, Xiao X, Xia L, Li W, Dong Y. Relationship between the widths of supercooled liquid regions and bond parameters of Mg-based bulk metallic glasses. J Non-Cryst Solids. 2003;321:120-5.

[16] Ye YF, Wang Q, Lu J, Liu CT, Yang Y. Design of high entropy alloys: A single-parameter thermodynamic rule. Scripta Mater. 2015;104:53-5.

[17] Ye YF, Liu CT, Yang Y. A geometric model for intrinsic residual strain and phase stability in high entropy alloys. Acta Mater. 2015;94:152-61.

[18] Wang ZJ, Qiu WF, Yang Y, Liu CT. Atomic-size and lattice-distortion effects in newly developed high-entropy alloys with multiple principal elements. Intermetallics. 2015;64:63-9.

[19] King DJM, Middleburgh SC, McGregor AG, Cortie MB. Predicting the formation and stability of single phase high-entropy alloys. Acta Mater. 2016;104:172-9.

[20] Troparevsky MC, Morris JR, Kent PRC, Lupini AR, Stocks GM. Criteria for Predicting the Formation of Single-Phase High-Entropy Alloys. Phys Rev X. 2015;5:011041.

[21] Senkov ON, Miracle DB. A new thermodynamic parameter to predict formation of solid solution or intermetallic phases in high entropy alloys. J Alloys Compd. 2016;658:603-7.

[22] Poletti MG, Battezzati L. Electronic and thermodynamic criteria for the occurrence of high entropy alloys in metallic systems. Acta Mater. 2014;75:297-306.

[23] Toda-Caraballo I, Rivera-Diaz-del-Castillo PEJ. A criterion for the formation of high entropy alloys based on lattice distortion. Intermetallics. 2016;71:76-87.

[24] Zhang Y, Guo S, Liu CT, Yang X. Phase Formation Rules. In: Gao MC, Yeh JW, Liaw PK, Zhang Y, editors. High-Entropy Alloys: Fundamentals and Applications. 1st ed. Cham, Switzerland: Springer International Publishing; 2016. p. 21-50.

[25] Pearson WB. Crystal chemistry and physics of metals and alloys. Phys Today. 1972;26:59.

[26] Kaufman L. Computer Calculation of Phase Diagrams. New York: Academic Press; 1970.

[27] Chang YA, Chen SL, Zhang F, Yan XY, Xie FY, Schmid-Fetzer R, et al. Phase diagram calculation: past, present and future. Prog Mater Sci. 2004;49:313-45.

[28] Pandat™. Thermodynamic Calculations and Kinetic Simulations. Madison, WI 53562 , USA: CompuTherm LLC.

[29] ThermoCalc. www.thermocalc.com.

[30] Zhang C, Zhang F, Chen SL, Cao WS. Computational Thermodynamics Aided High-Entropy Alloy Design. JOM. 2012;64:839-45.

[31] Zhang F, Zhang C, Chen SL, Zhu J, Cao WS, Kattner UR. An understanding of high entropy alloys from phase diagram calculations. CALPHAD. 2014;45:1-10.

[32] Senkov ON, Miller JD, Miracles DB, Woodward C. Accelerated exploration of multi-principal element alloys for structural applications. CALPHAD. 2015;50:32-48.

[33] Zhang C, Gao MC. CALPHAD Modeling of High-Entropy Alloys. In: Gao MC, Yeh JW, Liaw PK, Zhang Y, editors. High-Entropy Alloys: Fundamentals and Applications. 1st ed. Cham: Springer International Publishing; 2016. p. 399-444.

[34] Zhang C, Zhang F, Diao H, Gao MC, Tang Z, Liaw PK. Understanding Phase Stability of Al-Co-Cr-Fe-Ni High Entropy Alloys. Mater Des. 2016;109:425-33.

[35] Daoud HM, Manzoni AM, Wanderka N, Glatzel U. High-Temperature Tensile Strength of Al10Co25Cr8Fe15Ni36Ti6 Compositionally Complex Alloy (High-Entropy Alloy). JOM. 2015;in press.

[36] Tian FY, Varga LK, Chen NX, Delczeg L, Vitos L. Ab initio investigation of high-entropy alloys of 3d elements. Phys Rev B. 2013;87:075144.

[37] Widom M, Huhn WP, Maiti S, Steurer W. Hybrid Monte Carlo/Molecular Dynamics Simulation of a Refractory Metal High Entropy Alloy. Metall Mater Trans A. 2014;45A:196-200.

[38] Zhang YW, Stocks GM, Jin K, Lu CY, Bei HB, Sales BC, et al. Influence of chemical disorder on energy dissipation and defect evolution in concentrated solid solution alloys. Nature Comm. 2015;6.

[39] Middleburgh SC, King DM, Lumpkin GR. Atomic scale modelling of hexagoal structured metallic fission product alloys. R Soc open Sci 2015;2:140292.

[40] Widom M. Prediction of structure and phase transformations. In: Gao MC, Yeh JW, Liaw PK, Zhang Y, editors. High-Entropy Alloys: Fundamentals and Applications. 1st ed. Cham, Switzerland: Springer International Publishing; 2016. p. 267-98.

[41] Gao MC, Niu C, Jiang C, Irving DL. Applications of Special Quasi-Random Structures to High-Entropy Alloys. In: Gao MC, Yeh JW, Liaw PK, Zhang Y, editors. High-Entropy Alloys: Fundamentals and Applications. 1st ed. Cham, Switzerland: Springer International Publishing; 2016. p. 333-68.

[42] Tian FY, Varga LK, Shen J, Vitos L. Calculating elastic constants in high-entropy alloys using the coherent potential approximation: Current issues and errors. Comp Mater Sci. 2016;111:350-8.

[43] Miedema AR, de Boer FR, Boom R. Model predictions for the enthalpy of formation of transition metal alloys. CALPHAD. 1977;1:341-59.

[44] Otto F, Yang Y, Bei H, George EP. Relative effects of enthalpy and entropy on the phase stability of equiatomic high-entropy alloys. Acta Mater. 2013;61:2628-38.

[45] Otto F, Dlouhy A, Pradeep KG, Kubenova M, Raabe D, Eggeler G, et al. Decomposition of the single-phase high-entropy alloy CrMnFeCoNi after prolonged anneals at intermediate temperatures. Acta Mater. 2016;112:40-52.

[46] Lucas MS, Wilks GB, Mauger L, Munoz JA, Senkov ON, Michel E, et al. Absence of long-range chemical ordering in equimolar FeCoCrNi. Appl Phys Lett. 2012;100:251907-4.

[47] Wu Z, Bei H, Otto F, Pharr GM, George EP. Recovery, recrystallization, grain growth and phase stability of a family of FCC-structured multi-component equiatomic solid solution alloys. Intermetallics. 2014;46:131-40.

[48] Tong CJ, Chen YL, Chen SK, Yeh JW, Shun TT, Tsau CH, et al. Microstructure characterization of AlxCoCrCuFeNi high-entropy alloy system with multiprincipal elements. Metall Mat Trans A. 2005;36A:881-93.

[49] Singh S, Wanderka N, Murty BS, Glatzel U, Banhart J. Decomposition in multi-component AlCoCrCuFeNi high-entropy alloy. Acta Mater. 2011;59:182-90.

[50] Chuang MH, Tsai MH, Wang WR, Lin SJ, Yeh JW. Microstructure and wear behavior of Al(x)Co(1.5)CrFeNi(1.5)Ti(y) high-entropy alloys. Acta Mater. 2011;59:6308-17.

[51] Kao YF, Chen TJ, Chen SK, Yeh JW. Microstructure and mechanical property of as-cast, -homogenized, and -deformed AlxCoCrFeNi (0 <= x <= 2) high-entropy alloys. J Alloys Compd. 2009;488:57-64.

[52] Wang WR, Wang WL, Yeh JW. Phases, microstructure and mechanical properties of Al_xCoCrFeNi high-entropy alloys at elevated temperatures. J Alloys Compds. 2014;589:143-52.

[53] Park N, Watanabe I, Terada D, Yokoyama Y, Liaw PK, Tsuji N. Recrystallization Behavior of CoCrCuFeNi High-Entropy Alloy. Metall Mater Trans A. 2015;46A:1481-7.

[54] Liu WH, He JY, Huang HL, Wang H, Lu ZP, Liu CT. Effects of Nb additions on the microstructure and mechanical property of CoCrFeNi high-entropy alloys. Intermetallics. 2015;60:1-8.

[55] Liu WH, Lu ZP, He JY, Luan JH, Wang ZJ, Liu B, et al. Ductile CoCrFeNiMox high entropy alloys strengthened by hard intermetallic phases. Acta Mater. 2016;116:332-42.

[56] Stepanov ND, Shaysultanov DG, Salishchev GA, Tikhonovsky MA, Oleynik EE, Tortika AS, et al. Effect of V content on microstructure and mechanical properties of the $CoCrFeMnNiV_x$ high entropy alloys. J Alloys Compd. 2015;628:170-85.

[57] Dahlborg U, Cornide J, Calvo-Dahlborg M, Hansen TC, Fitch A, Leong Z, et al. Structure of some CoCrFeNi and CoCrFeNiPd multicomponent HEA alloys by diffraction techniques. J Alloys Compd. 2016;681:330-41.

[58] Shun TT, Chang LY, Shiu MH. Microstructures and mechanical properties of multiprincipal component CoCrFeNiTix alloys. Materials Science and Engineering a-Structural Materials Properties Microstructure and Processing. 2012;556:170-4.

[59] Tang Z, Gao MC, Diao HY, Yang TF, Liu JP, Zuo TT, et al. Aluminum Alloying Effects on Lattice Types, Microstructures, and Mechanical Behavior of High-Entropy Alloys Systems. JOM. 2013;65:1848-58.

[60] Fultz B. Vibrational thermodynamics of materials. Progress in Materials Science. 2010;55:247-352.

[61] Feng R, Gao MC, Lee CH, Mathes M, Zuo T, Chen SY, et al. Design of Light-Weight High-Entropy Alloys. Entropy. 2016;18:333.

[62] Kresse G, Hafner J. Ab initio molecular dynamics for liquid metals. Phys Rev B. 1993;47:558-61.

[63] Kresse G, Furthmüller J. Efficient iterative schemes for ab initio total-energy calculations using a plane-wave basis set. Phys Rev B. 1996;54:11169-86.

[64] Lucas MS, Mauger L, Munoz JA, Xiao Y, Sheets AO, Semiatin SL, et al. Magnetic and vibrational properties of high-entropy alloys. J Appl Phys. 2011;109:07E307.

[65] Lucas MS, Belyea D, Bauer C, Bryant N, Michel E, Turgut Z, et al. Thermomagnetic analysis of $FeCoCr_xNi$ alloys: Magnetic entropy of high-entropy alloys. J Appl Phys. 2013;113:17A923.

[66] Huhn WP, Widom M. Prediction of A2 to B2 Phase Transition in the High-Entropy Alloy Mo-Nb-Ta-W. JOM. 2013;65:1772-9.

[67] Guggenheim EA. Statistical thermodynamics of mixtures with non-zero energies of mixing. Proc Roy Soc London A. 1944;183:213-27.

[68] Widom M. Entropy and Diffuse Scattering: Comparison of NbTiVZr and CrMoNbV. Metall Mater Trans A. 2016;47A:3306-11.

[69] Bethe HA. Statistical Theory of Superlattices. Proc Royal Soc London Ser A, Math Phys Sci. 1935;150:552-75.

[70] Ackermann H, Inden G, Kikuchi R. Tetrahedron approximation of the cluster variation method for bcc alloys. Acta Metall. 1989;37:1-7.

[71] Fultz B, Anthony L, Robertson JL, Nicklow RM, Spooner S, Mostoller M. Phonon modes and vibrational entropy of mixing in Fe-Cr. Physical Review B. 1995;52:3280-5.

[72] Nagel LJ, Anthony L, Fultz B. Differences in vibrational entropy of disordered and ordered Cu_3Au. Philosophical Magazine Letters. 1995;72:421-7.

[73] Zhang B, Gao MC, Zhang Y, Yang S, Guo SM. Senary Refractory High-Entropy Alloy MoNbTaTiVW. Mater Sci Tech. 2015;31:1207-13.

[74] Zhang B, Gao MC, Zhang Y, Guo SM. Senary Refractory High-Entropy Alloy Cr_xMoNbTaVW. CALPHAD. 2015;51:193-201.

[75] Gao MC, Zhang B, Yang S, Guo SM. Senary Refractory High-Entropy Alloy HfNbTaTiVZr. Metall Mater Trans A. 2016;47A:3333-45.

[76] Yao HW, Qiao JW, Gao MC, Hawk JA, Ma SG, Zhou HF, et al. NbTaV-(Ti, W) Refractory High Entropy Alloys. Mater Sci Eng A. 2016;674:203-11.

[77] Yao HW, Qiao JW, Gao MC, Hawk JA, Ma SG, Zhou HF. MoNbTaV Medium-Entropy Alloy. Entropy. 2016;18:189.

[78] Senkov ON, Miller JD, Miracle DB, Woodward C. Accelerated exploration of multi-principal element alloys with solid solution phases. Nature Comm. 2015;6:6529.

[79] Scheil E. Comments on the layer crystal formation. Z Metallkd. 1942;34:70-2.

[80] Tang Z, Senkov ON, Parish CM, Zhang C, Zhang F, Santodonato LJ, et al. Tensile ductility of an AlCoCrFeNi multi-phase high-entropy alloy through hot isostatic pressing (HIP) and homogenization. Mater Sci Engin A. 2015;647:229-40.

[81] Chou KC, Chang YA. A Study of Ternary Geometrical Models. Ber Bunsenges Phys Chem. 1989;93:735-41.

[82] Pickering EJ, Munoz-Moreno R, Stone HJ, Jones NG. Precipitation in the equiatomic high-entropy alloy CrMnFeCoNi. Scripta Mater. 2016;113:106-9.

[83] Mihalkovič M, Widom M. Ab initio calculations of cohesive energies of Fe-based glass-forming alloys. Phys Rev B. 2004;70:144107.

[84] Gao MC, Unlu N, Shiflet GJ, Mihalkovic M, Widom M. Reassessment of Al-Ce and Al-Nd binary systems supported by critical experiments and first-principles energy calculations. Metall Mater Trans A. 2005;36A:3269-79.

[85] Ghosh G, Asta M. First-principles calculation of structural energetics of Al-TM (TM = Ti, Zr, Hf) intermetallics. Acta Mater. 2005;53:3225-52.

[86] Sluiter MHF. Ab initio lattice stabilities of some elemental complex structures. CALPHAD. 2006;30:357-66.

[87] Gao MC, Rollett AD, Widom M. First-principles calculation of lattice stability of C15-M2R and their hypothetical C15 variants (M = Al, Co, Ni; R = Ca, Ce, Nd, Y). CALPHAD. 2006;30:341-8.

[88] Curtarolo S, Setyawan W, Hart GLW, Jahnatek M, Chepulskii RV, Taylor RH, et al. AFLOW: An automatic framework for high-throughput materials discovery. Comp Mater Sci. 2012;58:218-26.

[89] Gao MC, Rollett AD, Widom M. The Lattice Stability of Aluminum-Rare Earth Binary Systems: A First Principles Approach. Phys Rev B. 2007;75:174120.

[90] Jablonksi PD, Licavoli J, Gao MC, Hawk JA. Manufacturing of High Entropy Alloys. JOM. 2015;67:2278-87.

[91] Zhang F, Cao W, Chen SL, Zhang C, Zhu J. In: Li M, Campbell C, Thornton K, Holm E, Gumbsch P, editors. the 2nd World Congress on Integrated Computational Materials Engineering (ICME). Salt Lake City, Utah, USA: TMS; 2013. p. 195-200.

Figure Caption

Figure 1. Comparison of various empirical parameters in separating single-phase alloys from multiphase alloys and amorphous alloys.

Figure 2. Calculated isopleths of (a) $CoFeMnNiCr_x$, (b) $CoCrFeMnNi_x$, (c) $CoCrFeNiAl_x$, and (d) $CoCrFeNiCu_x$, using the PanHEA database.

Figure 3. Calculated driving force contours [J/mol] of the σ phase nucleating from the FCC phase within the (a) $CoCr_x$, (b) $CoFeCr_x$, (c) $CoFeMnCr_x$, and (d) $CoFeMnNiCr_x$ systems using the PanHEA database, overlaid with the corresponding phase diagrams.

Figure 4. Calculated total entropy for the BCC, FCC, HCP, and σ phases for different alloys using the PanHEA database: (a) CoCr; (b) CoCrFe; (c) CoCrFeMn; (d) CoCrFeMnNi

Figure 5. Calculated entropy of mixing ($\Delta S_{\text{mix}}^{BCC}$) and enthalpy of mixing ($\Delta H_{\text{mix}}^{BCC}$) of the BCC solid-solution phase at 1273 K using the TCNI8 database: (a, b) $AlTi_x$, $AlVTi_x$, $AlNbVTi_x$ and $AlCrNbVTi_x$; (c, d) $CrTi_x$, $CrVTi_x$, $CrNbVTi_x$ and $CrNbVZrTi_x$ systems. The reference state is the BCC phase at 1273 K and 1 atm. The dashed curves in (a) and (c) refer to the ideal configurational entropies.

Figure 6. DFT-calculated enthalpy of formation of various single-phase CSSA in the FCC (blue), BCC (green) and HCP (red) structures.

Figure 7. Calculated (a) vibrational entropy, (b) electronic entropy, (c) configurational entropy, and (d) total entropy of FCC CoCrFeNi, BCC MoNbTaW, and HCP CoOsReRu, using DFT and MC/MD methods.

Figure 8. Calculated (a) vibrational entropy of mixing, (b) electronic entropy of mixing, and (c) total entropy of mixing for FCC CoCrFeNi, BCC MoNbTaW, and HCP CoOsReRu, using DFT and MC/MD methods.

empirical parameters

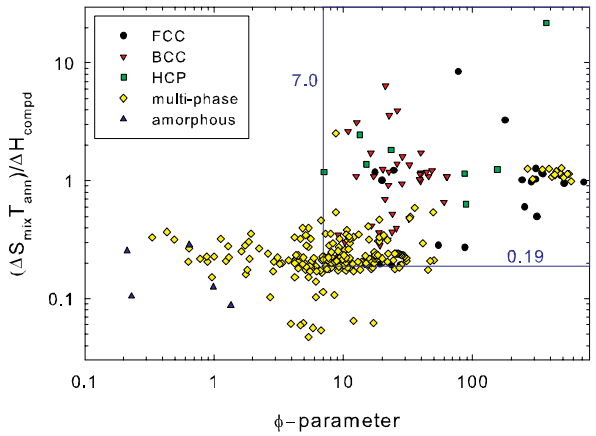

configurational entropy

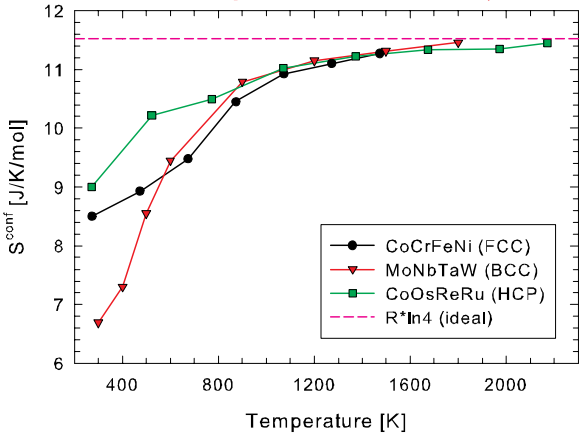

vibrational entropy of mixing

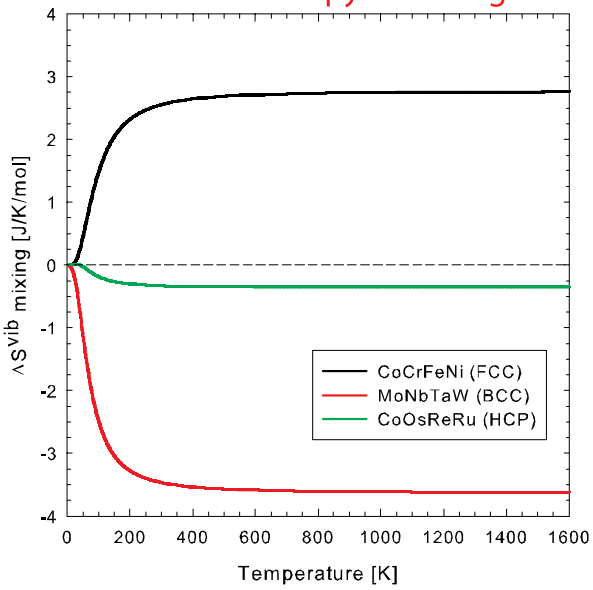

total entropy of mixing

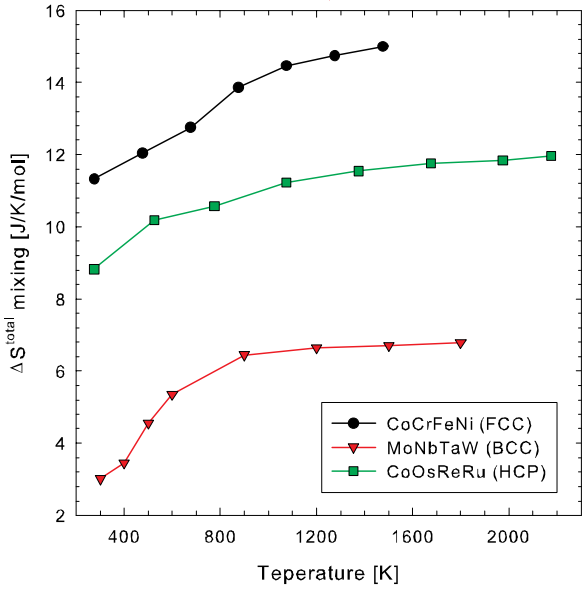

Figure 1.

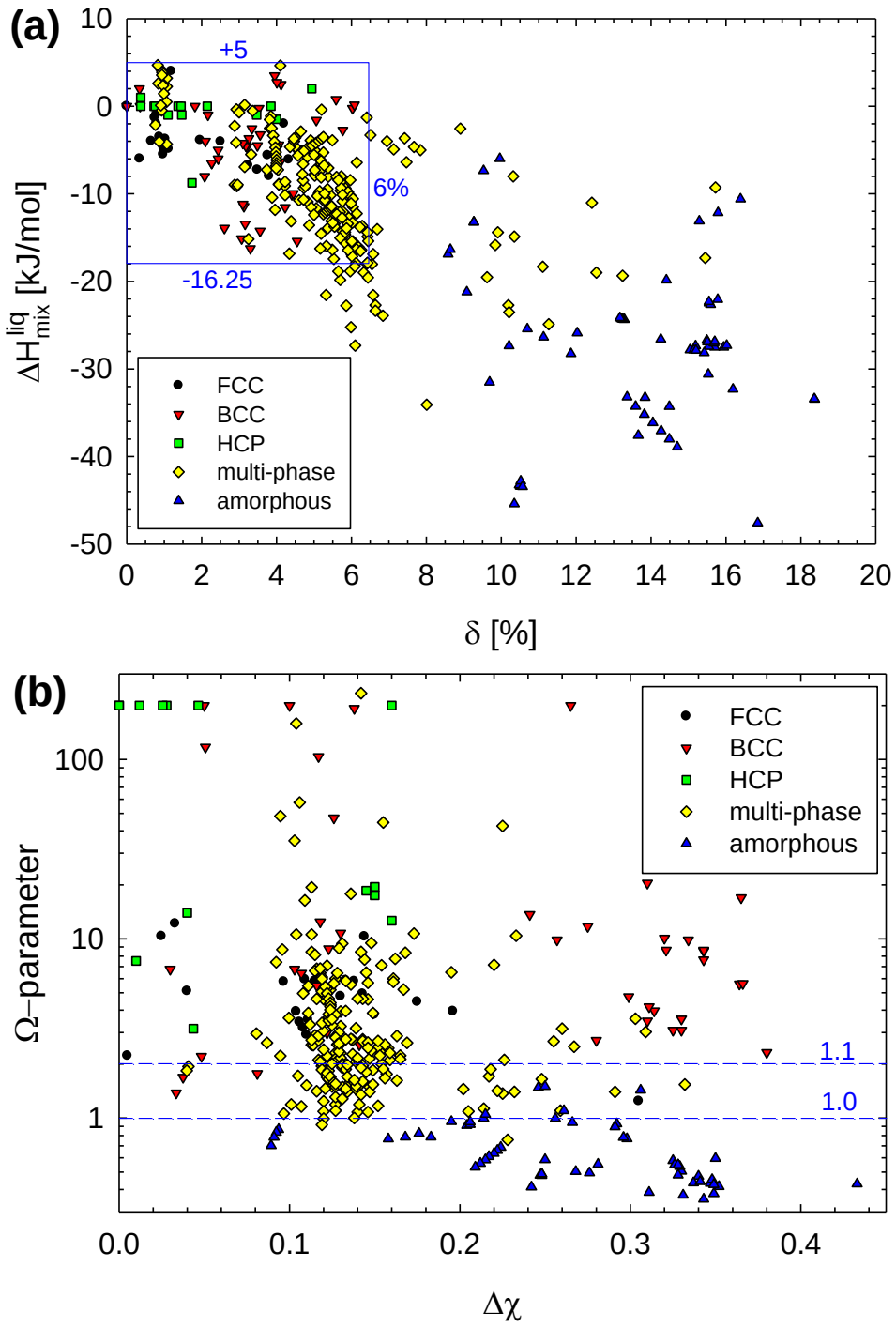
(a)
+5
6%
-16.25
FCC
BCC
HCP
multi-phase
amorphous
ΔH_{mix}^{liq} [kJ/mol]
δ [%]
(b)
FCC
BCC
HCP
multi-phase
amorphous
1.1
1.0
Ω–parameter
Δχ

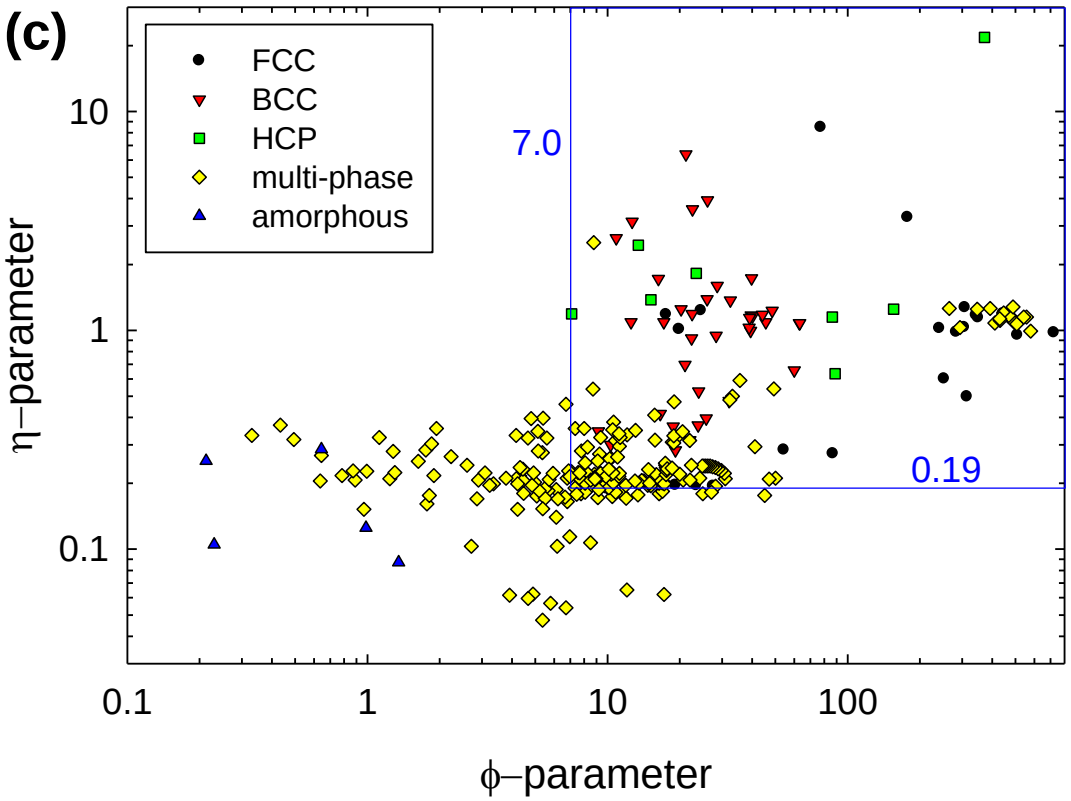
(c)
FCC
BCC
HCP
multi-phase
amorphous
7.0
0.19
η–parameter
ϕ–parameter
10
1
0.1
0.1
1
10
100

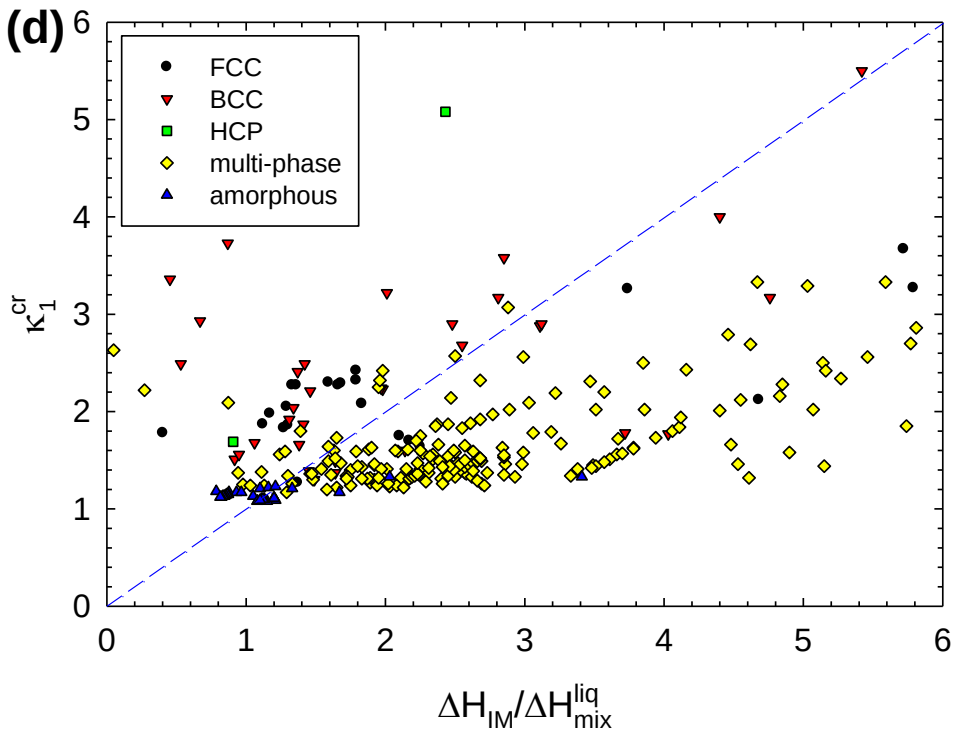
(d)
FCC
BCC
HCP
multi-phase
amorphous
κ_1^{cr}
$\Delta H_{IM}/\Delta H_{mix}^{liq}$
0
1
2
3
4
5
6

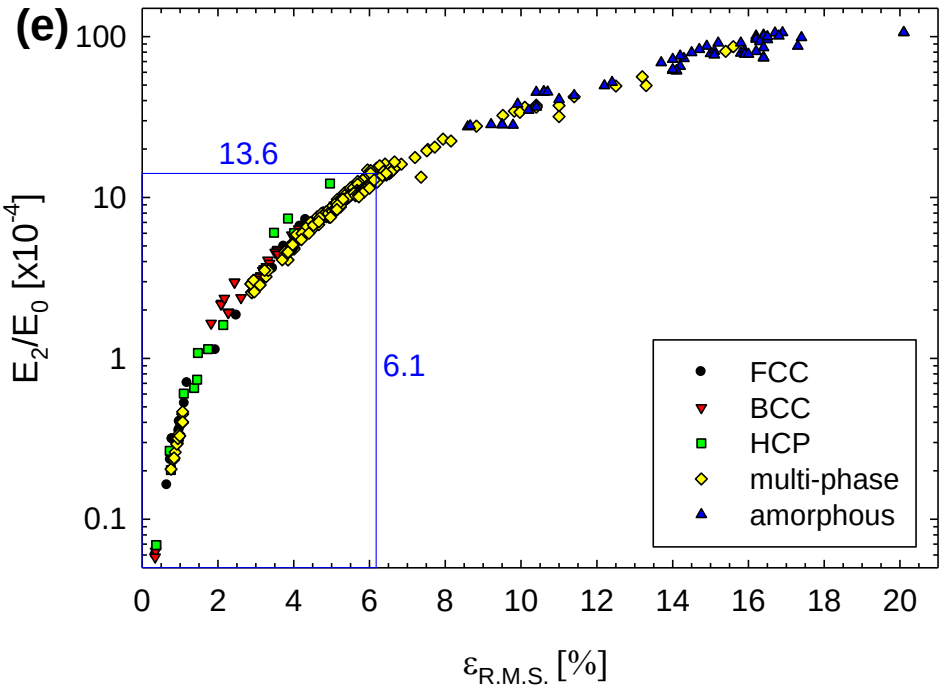
(e)
100
10
1
0.1
13.6
6.1
E_2/E_0 [x10^{-4}]
FCC
BCC
HCP
multi-phase
amorphous
0
2
4
6
8
10
12
14
16
18
20
$\varepsilon_{R.M.S.}$ [%]

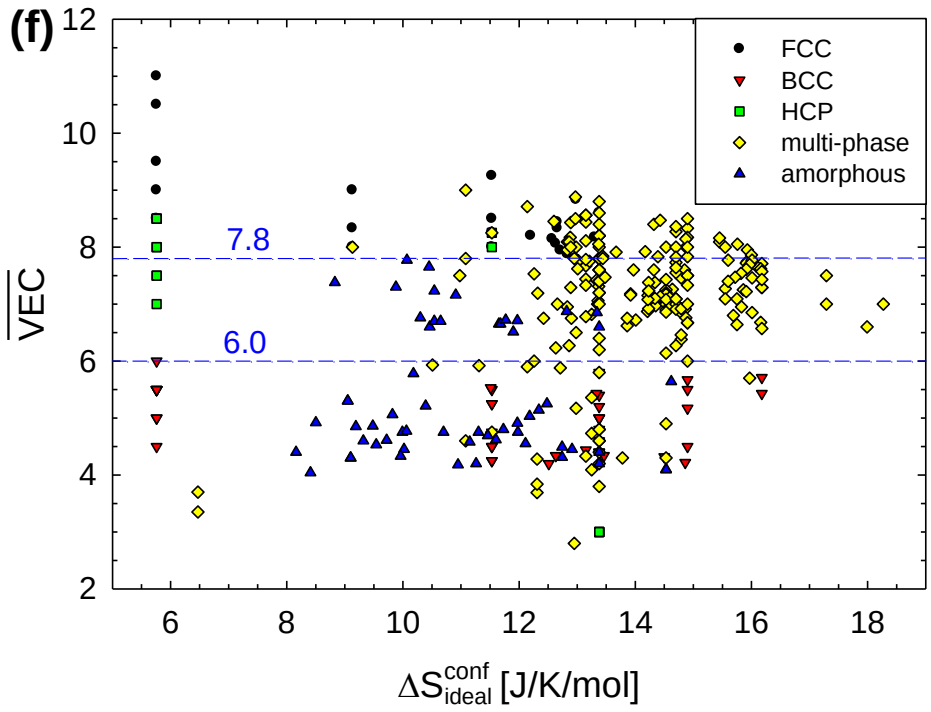
(f)
12
10
8
6
4
2
7.8
6.0
$\overline{VEC}$
FCC
BCC
HCP
multi-phase
amorphous
6
8
10
12
14
16
18
ΔS^{conf}_{ideal} [J/K/mol]

Figure 2.

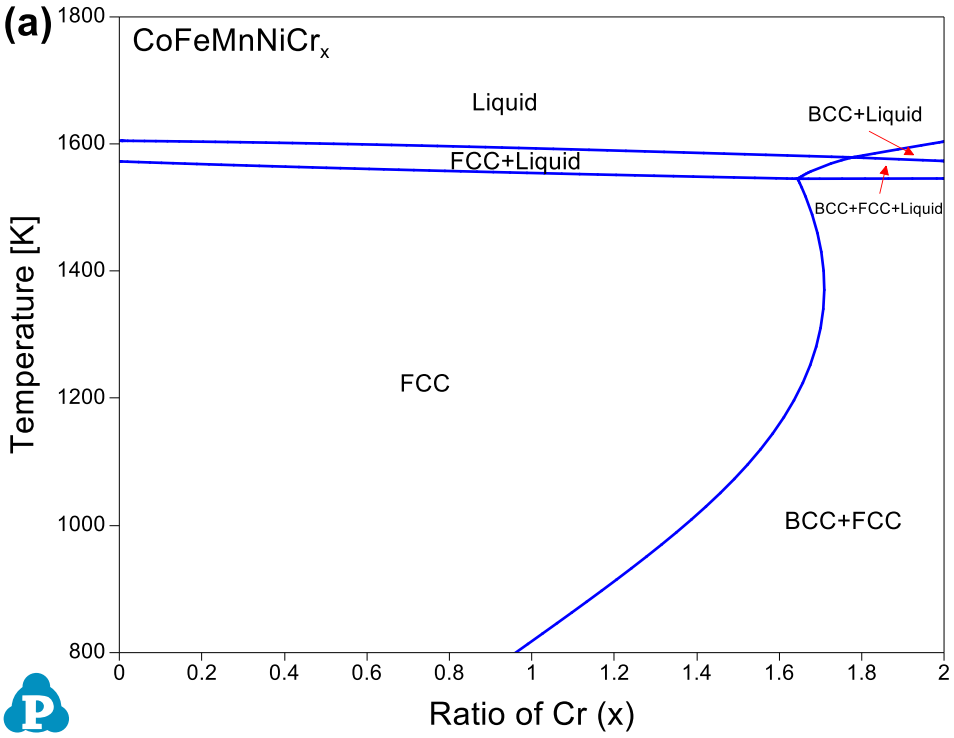
(a)
CoFeMnNiCrx
Liquid
BCC+Liquid
FCC+Liquid
BCC+FCC+Liquid
FCC
BCC+FCC
Temperature [K]
Ratio of Cr (x)
1800
1600
1400
1200
1000
800
0
0.2
0.4
0.6
0.8
1
1.2
1.4
1.6
1.8
2

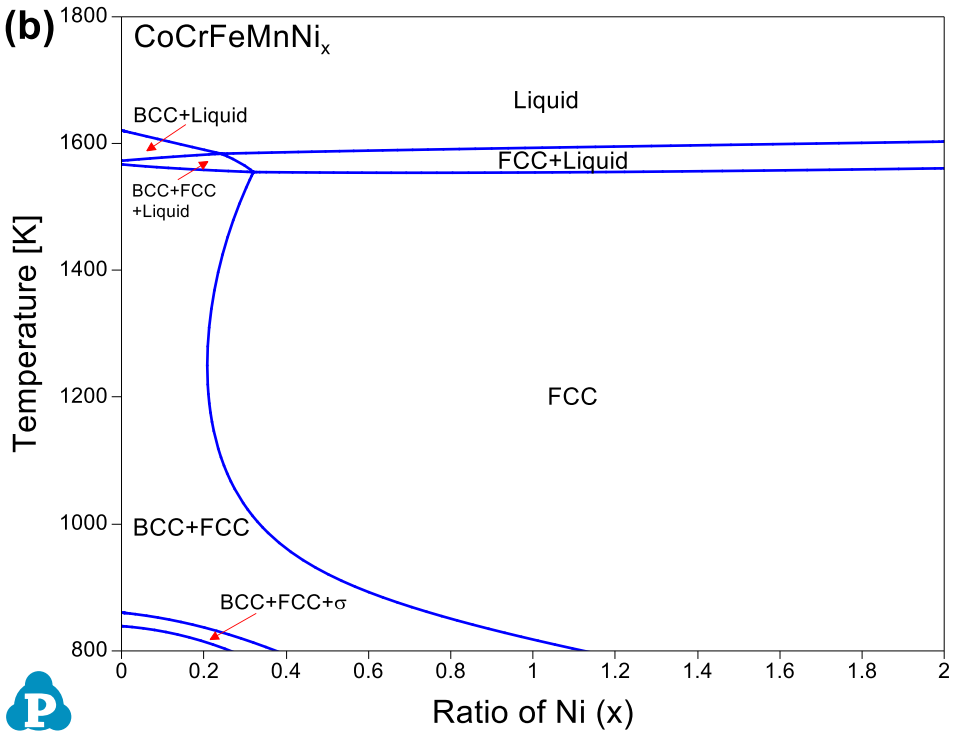
(b)
CoCrFeMnNix
Liquid
BCC+Liquid
FCC+Liquid
BCC+FCC
+Liquid
FCC
BCC+FCC
BCC+FCC+σ
Temperature [K]
Ratio of Ni (x)
1800
1600
1400
1200
1000
800
0
0.2
0.4
0.6
0.8
1
1.2
1.4
1.6
1.8
2

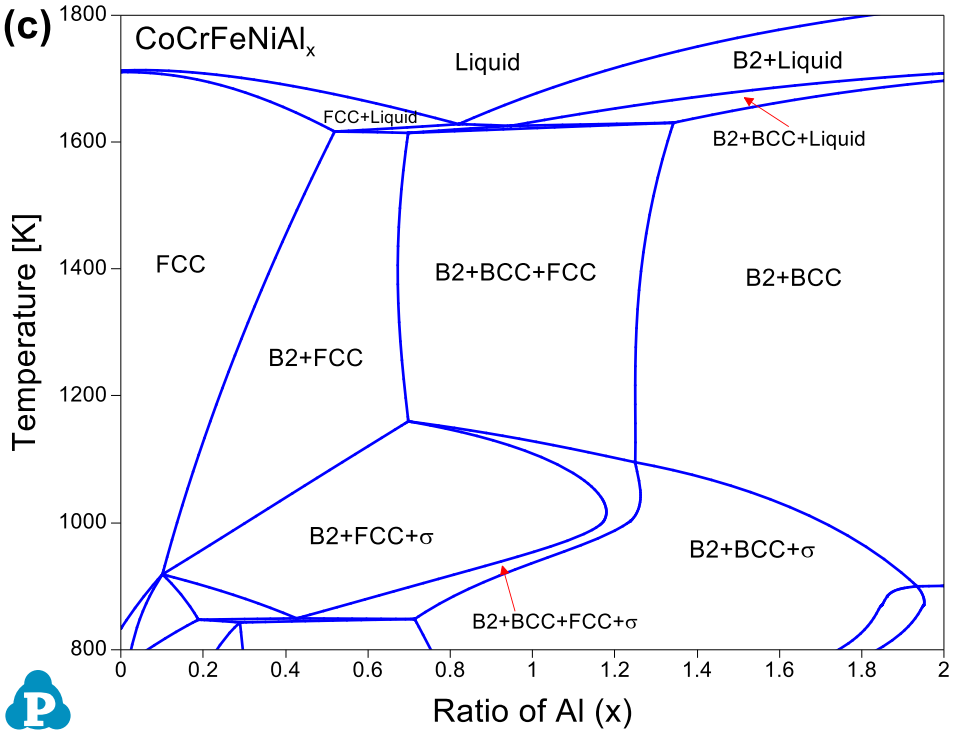
(c)
CoCrFeNiAl$_x$
Liquid
B2+Liquid
FCC+Liquid
B2+BCC+Liquid
FCC
B2+BCC+FCC
B2+BCC
B2+FCC
B2+FCC+σ
B2+BCC+σ
B2+BCC+FCC+σ
Temperature [K]
Ratio of Al (x)
1800
1600
1400
1200
1000
800
0
0.2
0.4
0.6
0.8
1
1.2
1.4
1.6
1.8
2

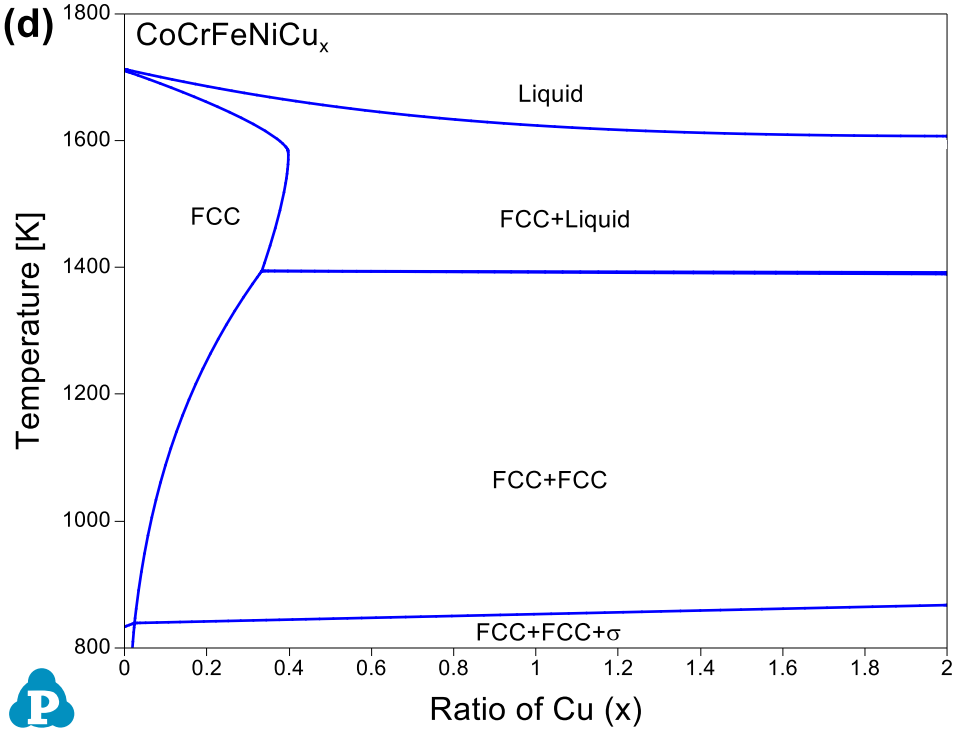
(d)
CoCrFeNiCu$_x$
Liquid
FCC
FCC+Liquid
FCC+FCC
FCC+FCC+σ
Temperature [K]
Ratio of Cu (x)
1800
1600
1400
1200
1000
800
0
0.2
0.4
0.6
0.8
1
1.2
1.4
1.6
1.8
2

Figure 3.

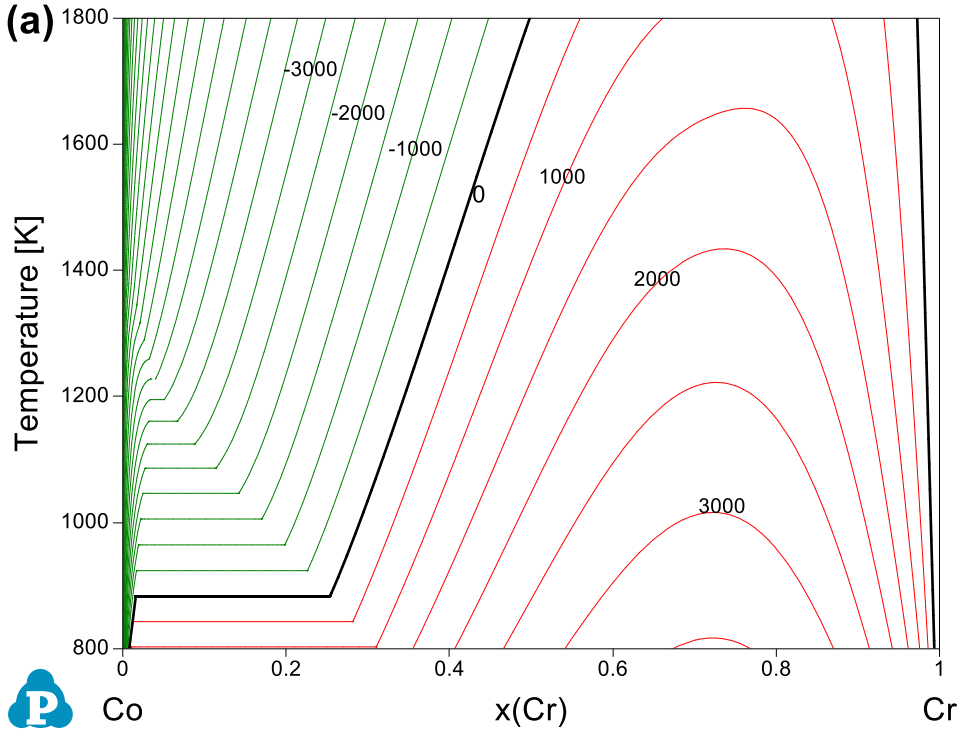
(a)
1800
1600
1400
1200
1000
800
Temperature [K]
-3000
-2000
-1000
0
1000
2000
3000
0
0.2
0.4
0.6
0.8
1
Co
x(Cr)
Cr

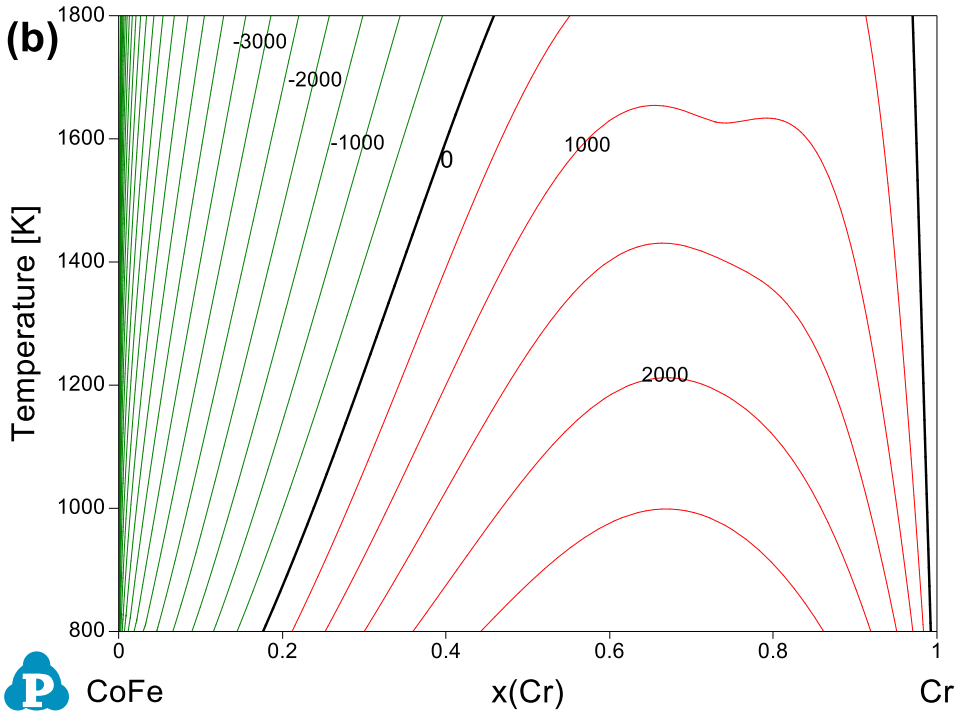
(b)
1800
1600
1400
1200
1000
800
Temperature [K]
-3000
-2000
-1000
0
1000
2000
0
0.2
0.4
0.6
0.8
1
CoFe
x(Cr)
Cr

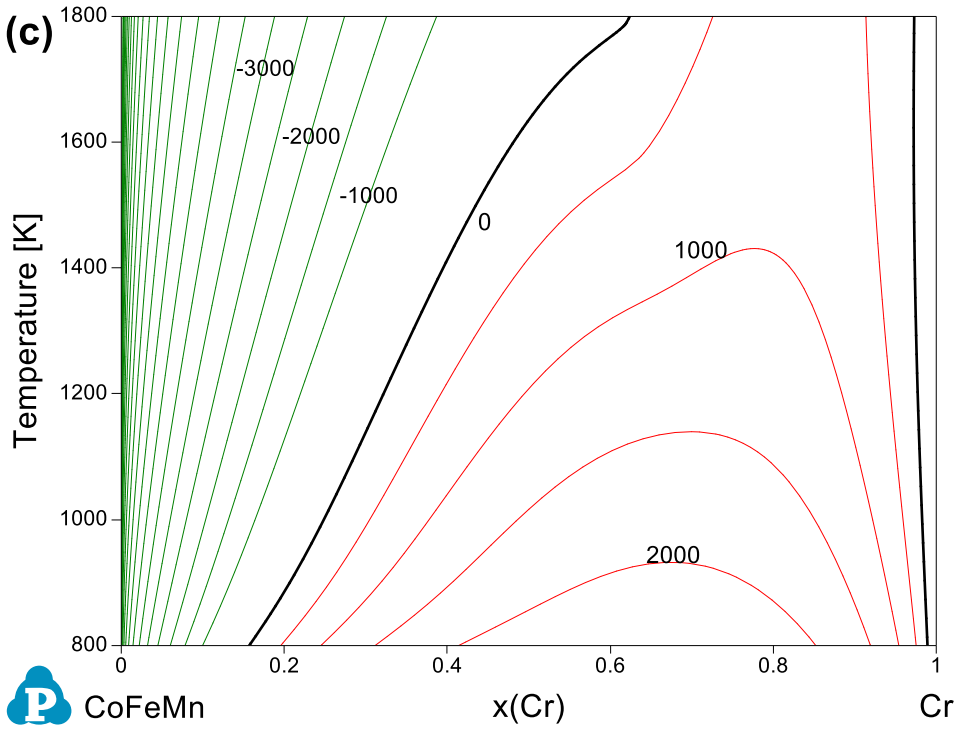
(c)
1800
1600
1400
1200
1000
800
Temperature [K]
-3000
-2000
-1000
0
1000
2000
0
0.2
0.4
0.6
0.8
1
CoFeMn
x(Cr)
Cr

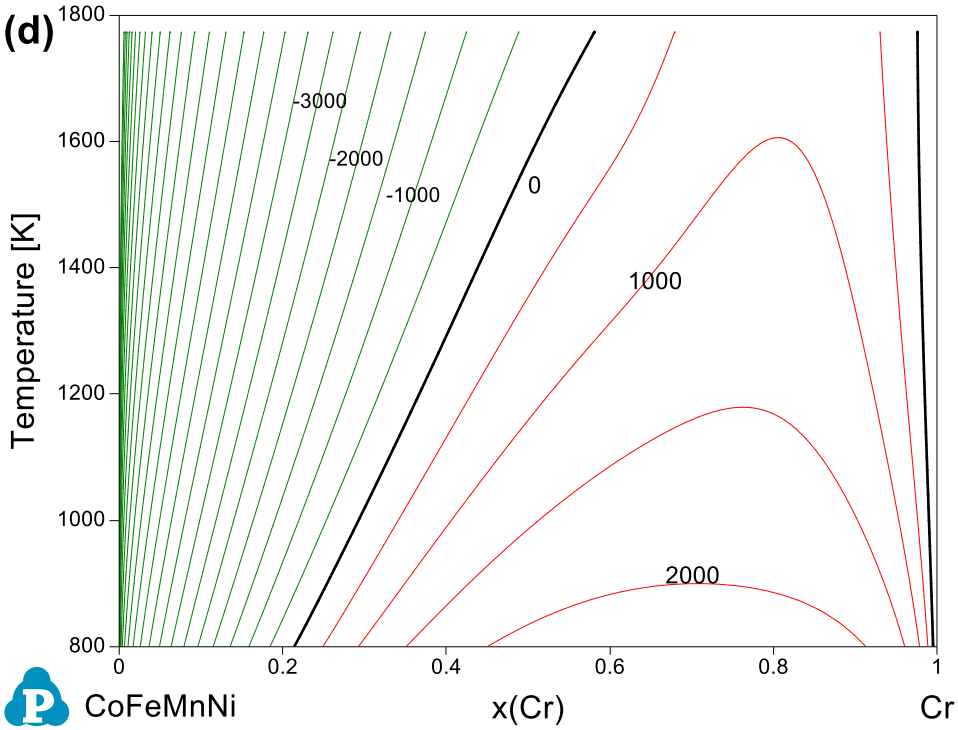
(d)
1800
1600
1400
1200
1000
800
Temperature [K]
-3000
-2000
-1000
0
1000
2000
0
0.2
0.4
0.6
0.8
1
CoFeMnNi
x(Cr)
Cr

Figure 4.

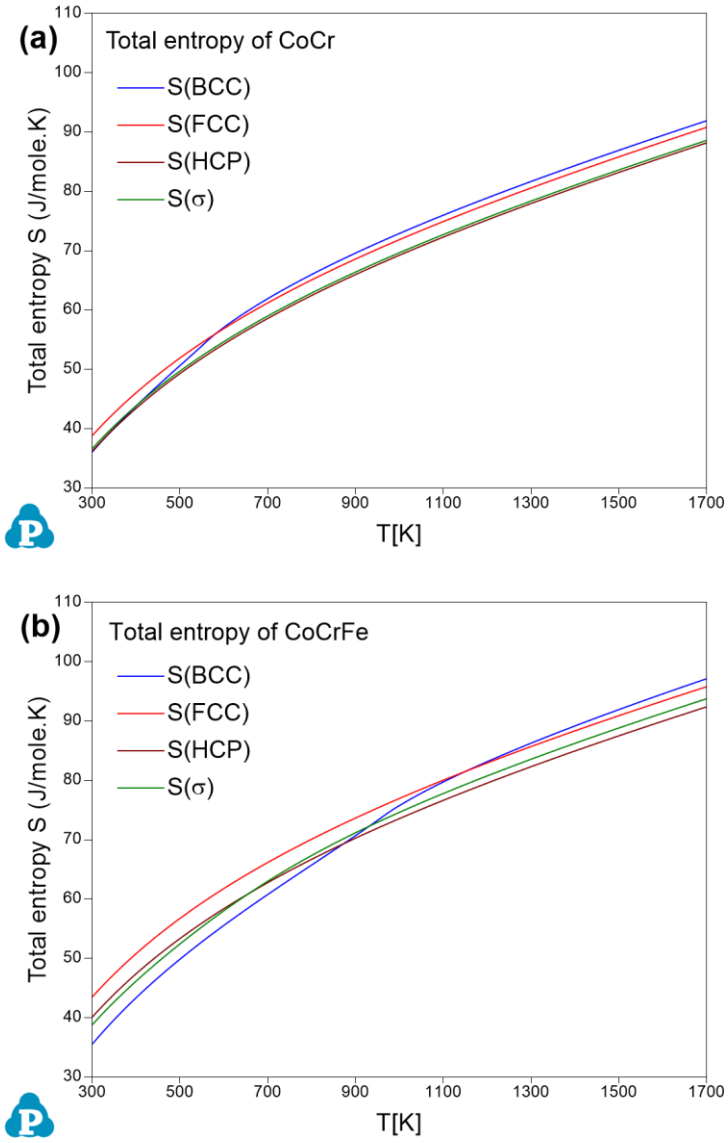
(a)
Total entropy of CoCr
S(BCC)
S(FCC)
S(HCP)
S(σ)
Total entropy S (J/mole.K)
T[K]
(b)
Total entropy of CoCrFe
S(BCC)
S(FCC)
S(HCP)
S(σ)
Total entropy S (J/mole.K)
T[K]

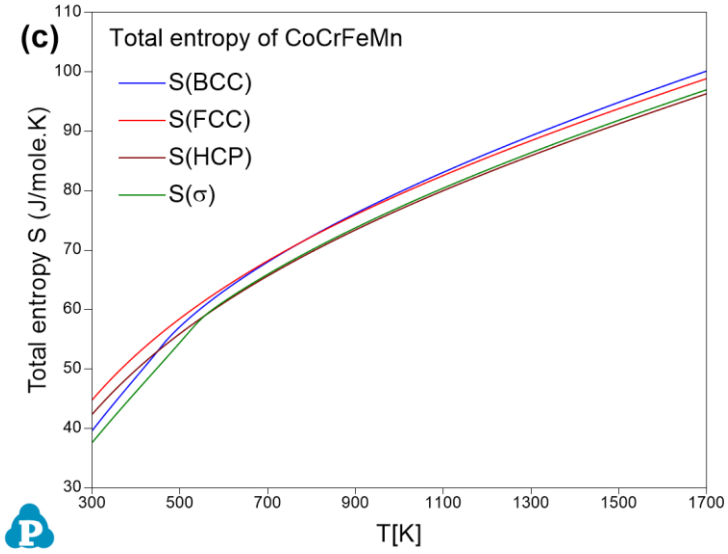
(c)
Total entropy of CoCrFeMn
S(BCC)
S(FCC)
S(HCP)
S(σ)
Total entropy S (J/mole.K)
T[K]
110
100
90
80
70
60
50
40
30
300
500
700
900
1100
1300
1500
1700

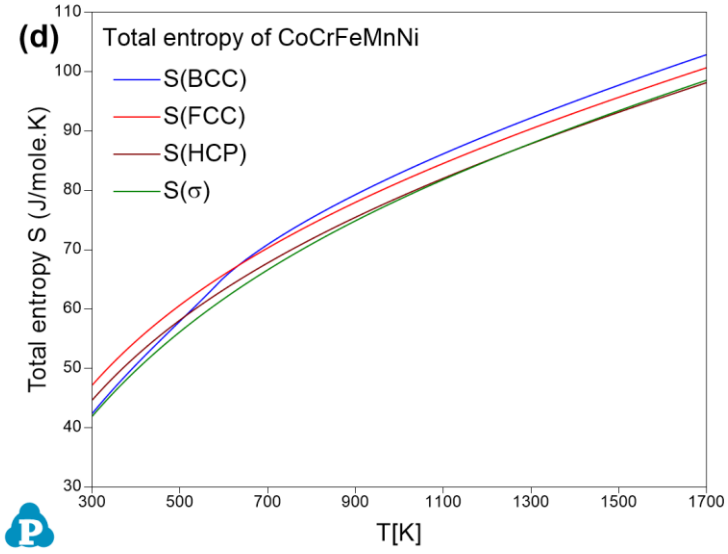
(d)
Total entropy of CoCrFeMnNi
S(BCC)
S(FCC)
S(HCP)
S(σ)
Total entropy S (J/mole.K)
T[K]
110
100
90
80
70
60
50
40
30
300
500
700
900
1100
1300
1500
1700

Figure 5.

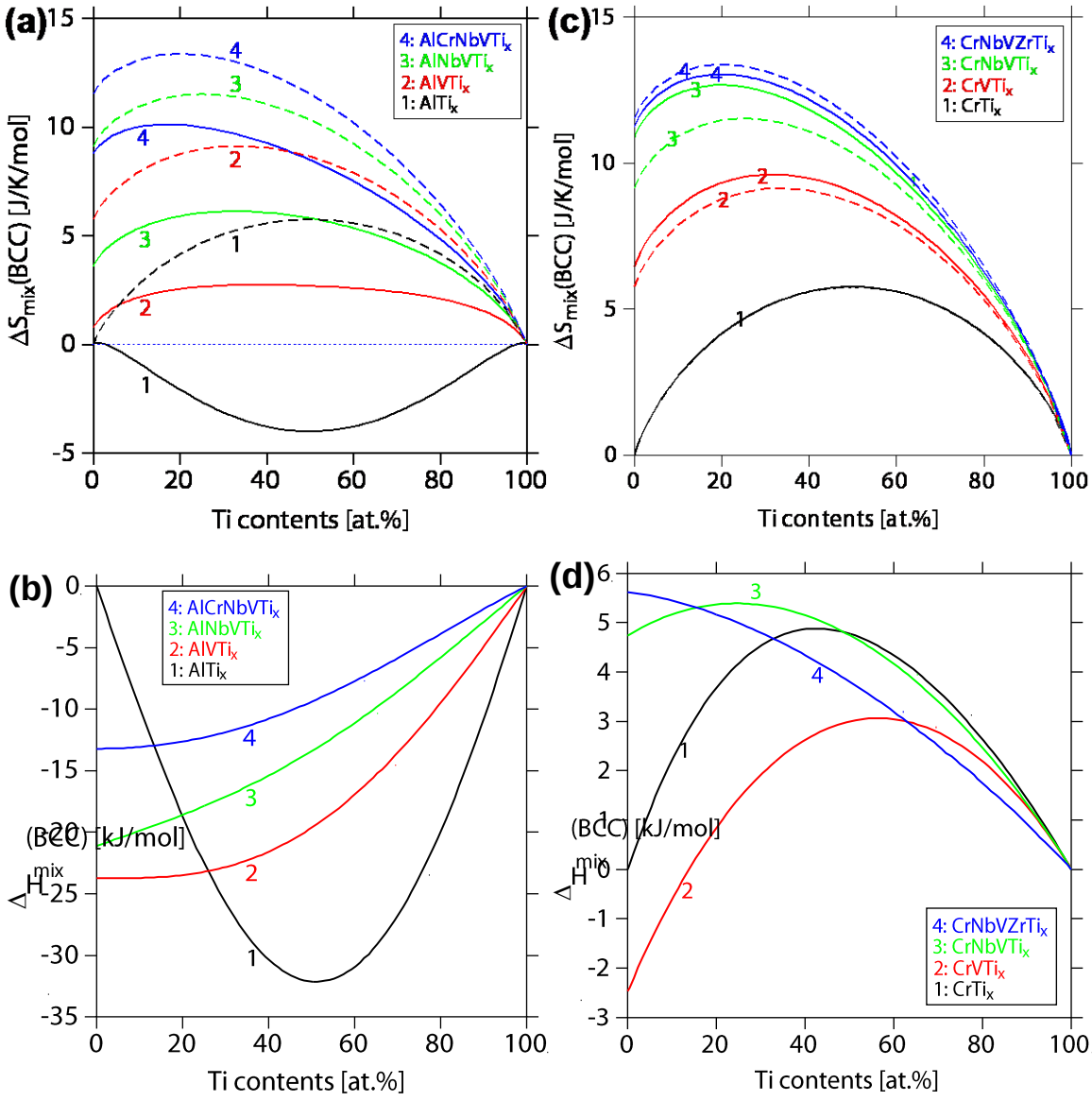
(a)
(c)
(b)
(d)
4: AlCrNbVTi$_x$
3: AlNbVTi$_x$
2: AlVTi$_x$
1: AlTi$_x$
4: CrNbVZrTi$_x$
3: CrNbVTi$_x$
2: CrVTi$_x$
1: CrTi$_x$
ΔS_{mix}(BCC) [J/K/mol]
ΔH_{mix}(BCC) [kJ/mol]
Ti contents [at.%]

Figure 6.

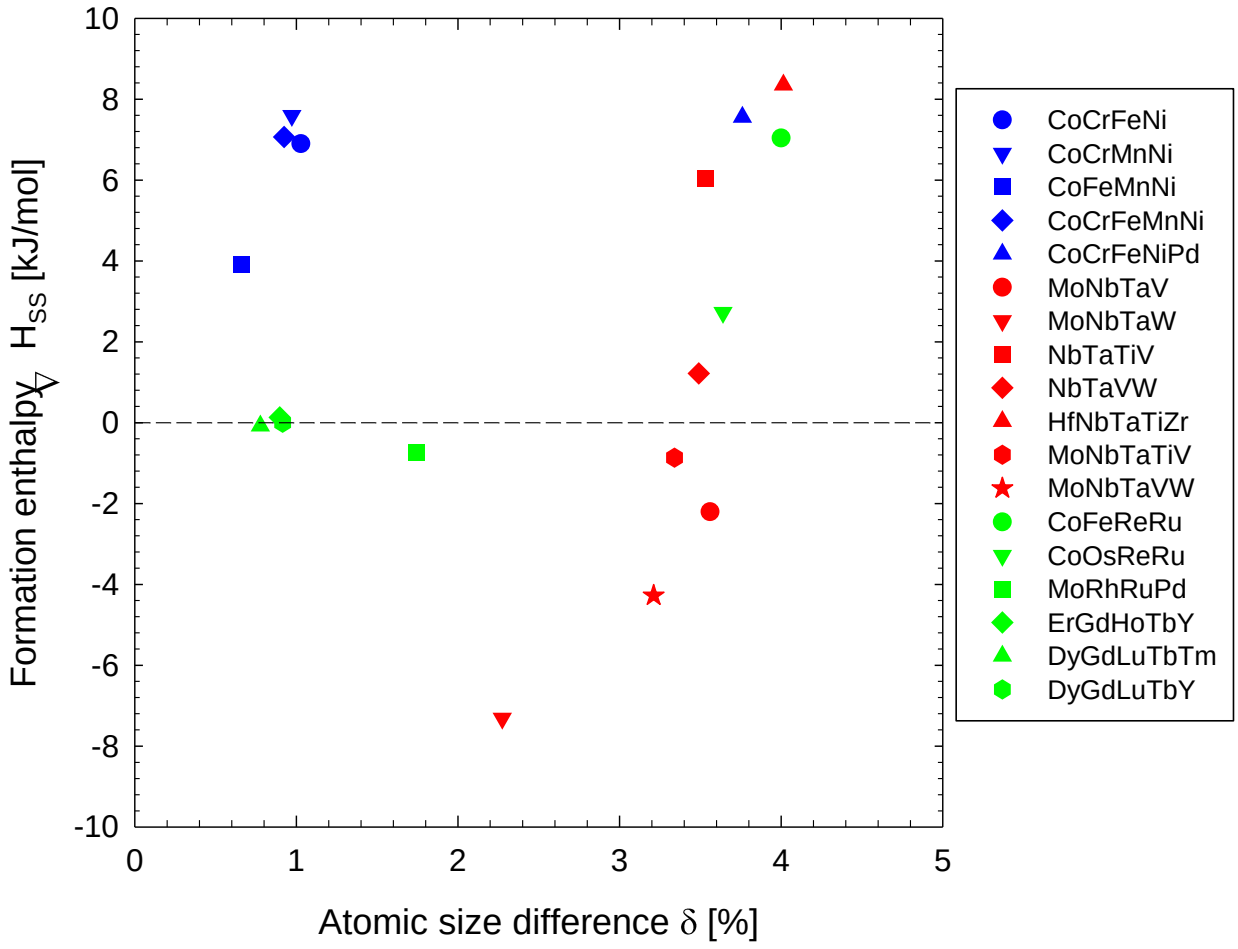
Formation enthalpy H_{SS} [kJ/mol]
Atomic size difference δ [%]
10
8
6
4
2
0
-2
-4
-6
-8
-10
0
1
2
3
4
5
CoCrFeNi
CoCrMnNi
CoFeMnNi
CoCrFeMnNi
CoCrFeNiPd
MoNbTaV
MoNbTaW
NbTaTiV
NbTaVW
HfNbTaTiZr
MoNbTaTiV
MoNbTaVW
CoFeReRu
CoOsReRu
MoRhRuPd
ErGdHoTbY
DyGdLuTbTm
DyGdLuTbY

Figure 7.

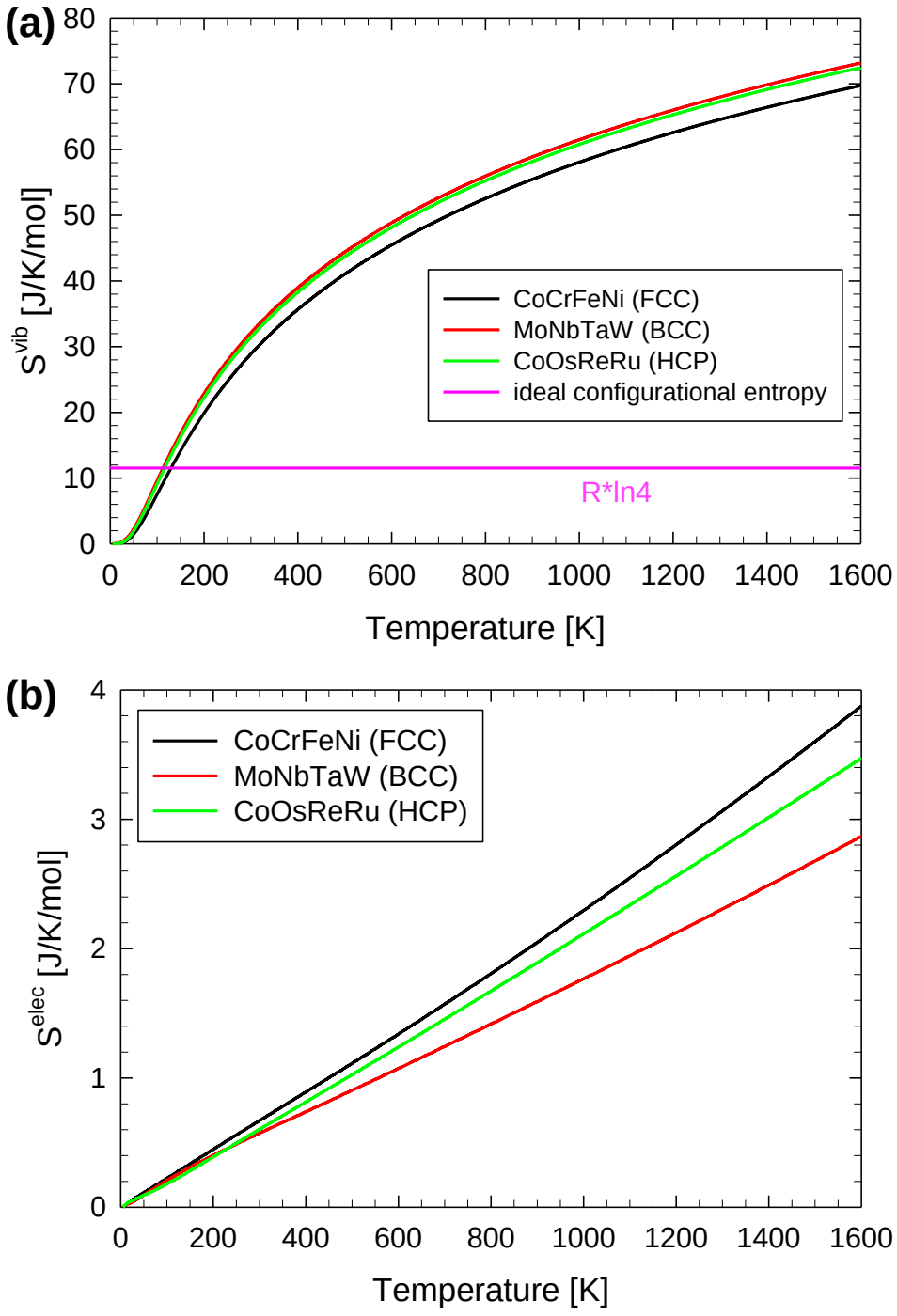
(a)
S^{vib} [J/K/mol]
Temperature [K]
CoCrFeNi (FCC)
MoNbTaW (BCC)
CoOsReRu (HCP)
ideal configurational entropy
R*ln4
(b)
S^{elec} [J/K/mol]
Temperature [K]
CoCrFeNi (FCC)
MoNbTaW (BCC)
CoOsReRu (HCP)

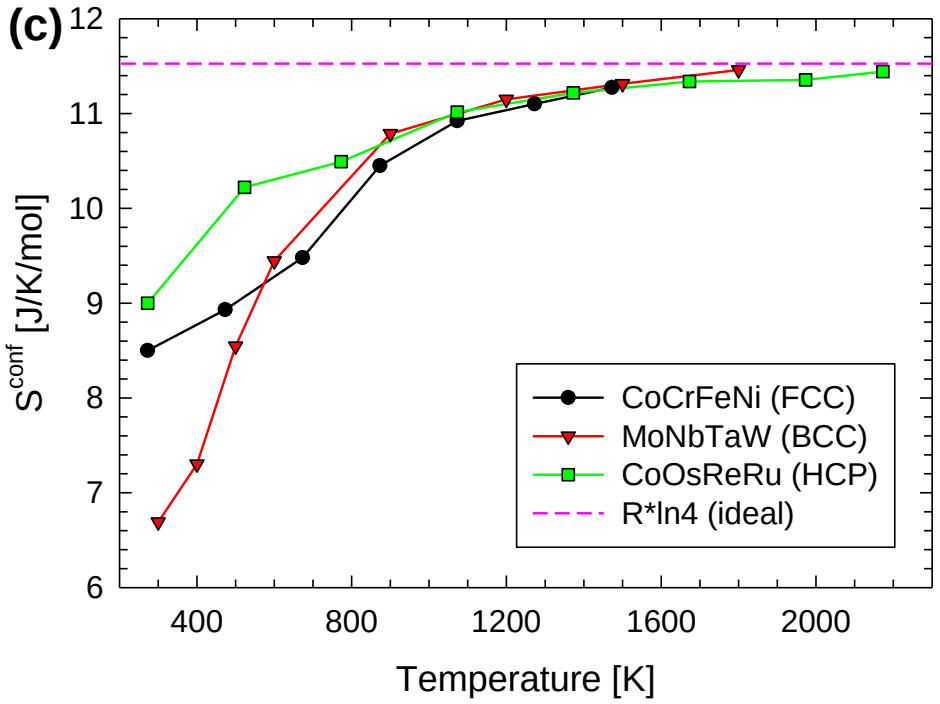
(c)
12
11
10
9
8
7
6
S^{conf} [J/K/mol]
400
800
1200
1600
2000
Temperature [K]
CoCrFeNi (FCC)
MoNbTaW (BCC)
CoOsReRu (HCP)
R*ln4 (ideal)

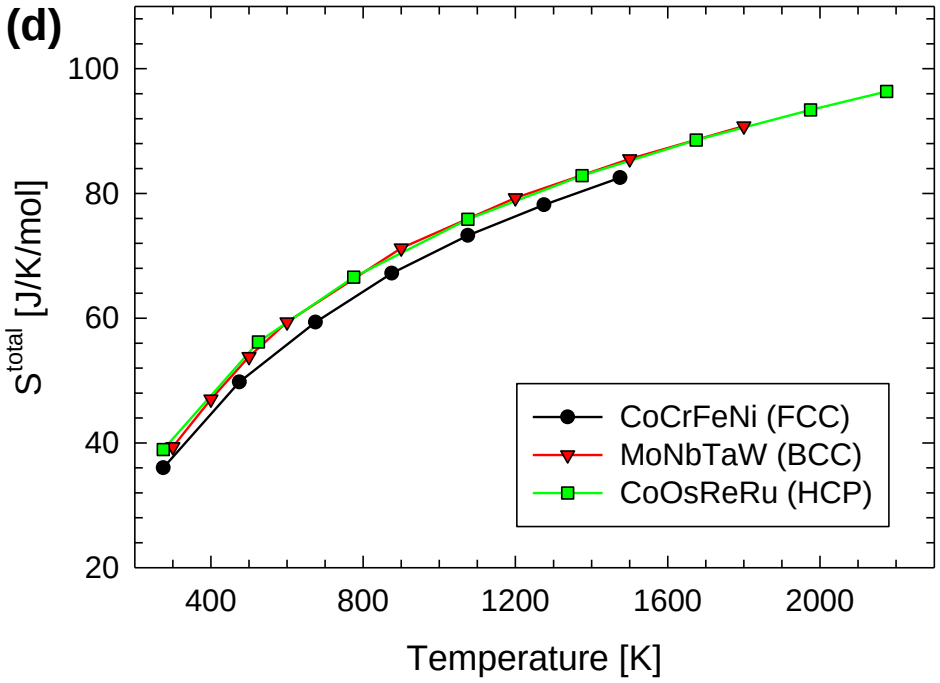
(d)
100
80
60
40
20
S^{total} [J/K/mol]
400
800
1200
1600
2000
Temperature [K]
CoCrFeNi (FCC)
MoNbTaW (BCC)
CoOsReRu (HCP)

Figure 8.

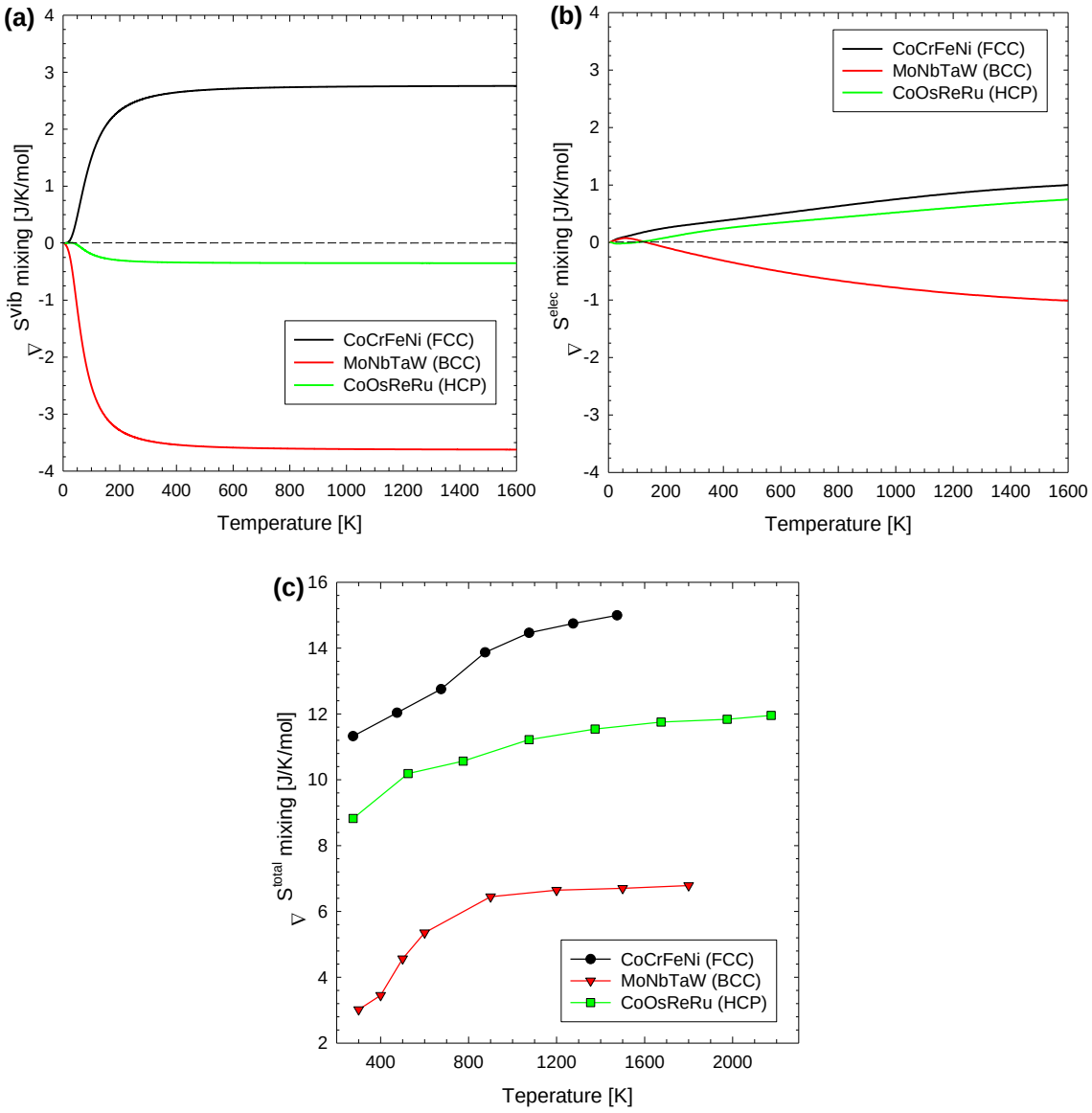
(a)
S^{vib} mixing [J/K/mol]
Temperature [K]
CoCrFeNi (FCC)
MoNbTaW (BCC)
CoOsReRu (HCP)
(b)
S^{elec} mixing [J/K/mol]
Temperature [K]
CoCrFeNi (FCC)
MoNbTaW (BCC)
CoOsReRu (HCP)
(c)
S^{total} mixing [J/K/mol]
Teperature [K]
CoCrFeNi (FCC)
MoNbTaW (BCC)
CoOsReRu (HCP)